Original Article

MOLECULAR METABOLISM

Knock-out of CD73 delays the onset of HR-negative breast cancer by reprogramming lipid metabolism and is associated with increased tumor mutational burden

Paweł Kamil Serafin[1,], Marta Popęda[2], Kamila Bulak[3], Agata Zwara[4], Barbara Galikowska-Bogut[5], Anna Przychodzka[5], Adriana Mika[4], Tomasz Śledziński[4], Marcin Stanisławowski[6], Kamila Jendernalik[7], Marika Bolcewicz[7], Wiktoria Laprus[1], Grzegorz Stasiłojć[1], Rafał Sądej[5], Anna Żaczek[8], Leszek Kalinowski[7,9], Patrycja Koszałka[1,*]**

ABSTRACT

Objective: CD73 (ecto-5′-nucleotidase, NT5E), a cell-surface enzyme converting 5′-AMP to adenosine, is crucial for cancer progression. However, its role in the tumorigenesis process remains mostly obscure. We aimed to demonstrate CD73's role in breast cancer (BC) tumorigenesis through metabolic rewiring of fatty acid metabolism, a process recently indicated to be regulated by BC major prognostic markers, hormone receptors (HR) for estrogen (ER), and progesterone (PR).

Methods: A murine model of chemically induced mammary gland tumorigenesis was applied to analyze CD73 knock-out (KO)-induced changes at the transcriptome (RNA-seq), proteome (IHC, WB), and lipidome (GC-EI-MS) levels. CD73 KO-induced changes were correlated with scRNA-seq and bulk RNA-seq data for human breast tissues and BCs from public collections and confirmed at the proteome level with IHC or WB analysis of BC tissue microarrays and cell lines.

Results: CD73 KO delayed the onset of HR/PR-negative mammary tumors in a murine model. This delay correlated with increased expression of genes related to biosynthesis and β-oxidation of fatty acids (FAs) in the CD73 KO group at the initiation stage. STRING analysis based on RNA-seq data indicated an interplay between CD73 KO, up-regulated expression of PR-coding gene, and DEGs involved in FA metabolism, with PPARγ, a main regulator of FA synthesis, as a main connective node. In epithelial cells of mammary glands, PPARγ expression correlated with CD73 at the RNA level. With cancer progression, CD73 KO increased the levels of PUFAn3/6 (polyunsaturated omega 3/6 FAs), known ligands of PPARγ and target for lipid peroxidation, which may lead to oxidative DNA damage. It correlated with the downregulation of genes involved in cellular stress response (*Mlh1*, *Gsta3*), PR—or CD73-dependent changes in the intracellular ROS levels and expression or activation of proteins involved in DNA repair or oxidative stress response in mammary tumor or human BC cell lines, increased tumor mutational burden (TMB) and genomic instability markers in CD73 low HR-negative human BCs, and the prolonged onset of tumors in the CD73 KO HR/PR-negative group.

[1]Laboratory of Cell Biology and Immunology, Institute of Medical Biotechnology and Experimental Oncology, Intercollegiate Faculty of Biotechnology University of Gdańsk and Medical University of Gdańsk, Medical University of Gdańsk, Poland [2]Department of Pathomorphology, Faculty of Medicine, Medical University of Gdańsk, Poland [3]Department of Pathomorphology and Forensic Veterinary Medicine, University of Life Sciences in Lublin, Poland [4]Department of Pharmaceutical Biochemistry, Medical University of Gdańsk, Poland [5]Laboratory of Molecular Enzymology and Oncology, Institute of Medical Biotechnology and Experimental Oncology, Intercollegiate Faculty of Biotechnology University of Gdańsk and Medical University of Gdańsk, Medical University of Gdańsk, Poland [6]Department of Histology, Faculty of Medicine, Medical University of Gdańsk, Poland [7]Department of Medical Laboratory Diagnostics—Fahrenheit Biobank BBMRI.pl, Faculty of Pharmacy, Medical University of Gdańsk, Poland [8]Laboratory of Translational Oncology, Institute of Medical Biotechnology and Experimental Oncology, Intercollegiate Faculty of Biotechnology University of Gdańsk and Medical University of Gdańsk, Medical University of Gdańsk, Poland [9]BioTechMed Centre, Department of Mechanics of Materials and Structures, Gdansk University of Technology, Gdansk, Poland

*Corresponding author. Laboratory of Cell Biology and Immunology, Institute of Medical Biotechnology and Experimental Oncology, Intercollegiate Faculty of Biotechnology University of Gdańsk and Medical University of Gdańsk, Medical University of Gdańsk, Dębinki Street 1, 80-211 Gdańsk, Poland. E-mail: patrycja.koszalka@gumed.edu.pl (P. Koszałka).

**Corresponding author. Laboratory of Cell Biology and Immunology, Institute of Medical Biotechnology and Experimental Oncology, Intercollegiate Faculty of Biotechnology University of Gdańsk and Medical University of Gdańsk, Medical University of Gdańsk, Dębinki Street 1, 80-211 Gdańsk, Poland. E-mail: pserafin@gumed.edu.pl (P.K. Serafin).

Abbreviations: BC, breast cancer; CAAI, complex arm-wise aberration index; CD73, cluster of differentiation 73, ecto-5′-nucleotidase; CD73 KO, CD73 knock-out; DSBs, DNA double-strand breaks; DDR, DNA damage response; DEGs, differentially expressed genes; DMBA, 7,12-dimethylbenz[a]anthracene; DMEM, Dulbecco's Modified Eagle's Medium; ER, estrogen receptor; FAs, fatty acids; GII, genomic instability index; HER2, human epidermal growth factor receptor 2; HR, hormone receptor; IntClust, integrative cluster; MPA, medroxyprogesterone acetate; NT5E/Nt5e, ecto-5′-nucleotidase gene; OS, overall survival; PPARγ/PPARG, peroxisome proliferator-activated receptor gamma; PR, progesterone receptor; PUFAn3/6, polyunsaturated omega-3/6 FAs; ROS, reactive oxygen species; MGs, mammary glands; MGTs, mammary gland tumors; TFS, tumor-free survival; TMB, tumor mutational burden; TNBC, triple-negative breast cancer; WT, wild-type

Received June 14, 2024 • Revision received September 16, 2024 • Accepted September 16, 2024 • Available online 18 September 2024

https://doi.org/10.1016/j.molmet.2024.102035

Conclusions: CD73 has a significant role in tumorigenesis driving the reprogramming of lipid metabolism through the regulatory loop with PR and PPARγ in epithelial cells of mammary glands. Low CD73 expression/CD73 KO might enhance mutational burden by disrupting this regulatory loop, delaying the onset of HR-negative tumors. Our results support combining therapy targeting the CD73-adenosine axis and tumor lipidome against HR-negative tumors, especially at their earliest developmental stage.

Keywords CD73; Breast cancer tumorigenesis; Progesterone receptor; Lipid metabolism; PPARγ; Tumor mutational burden

1. INTRODUCTION

CD73 (ecto-5′-nucleotidase, eNT, *NT5E*) is a widely expressed cell-surface enzyme preferentially catalyzing the conversion of 5′-AMP to extracellular adenosine and a main target of more than 15 phase I/II clinical trials for anti-cancer therapy [3]. In preclinical research, its depletion through genetic alterations or inhibition decreased the tumor growth and metastasis of many cancer types, including BC [4,5]. Through extracellular adenosine-regulated purinergic signaling, CD73 mediates several tissue-protective mechanisms, both physiological and pathological. Its expression and activity are upregulated as a part of an adaptive response to hypoxia or inflammation. In syngeneic or xenotransplant mouse models, CD73 was shown to favor the progression of neoplastic disease mainly through the generation of an immunosuppressed niche, stimulation of angiogenesis, cancer cell proliferation, and epithelial-to-mesenchymal transition [5,6]. Its depletion also reduced tumor incidence in the murine model of 3-methyl-cholanthrene-induced fibrosarcoma and delayed the onset of prostate cancer in TRAMP transgenic mice in correlation with its immunomodulatory activity [7].

However, for BC clinical data indicates a significant ambiguity about the correlation between CD73 expression and overall survival (OS), as well as the expression of its main clinical biomarkers, the expression of hormone receptors (HR) for estrogen (ER) and progesterone (PR), and amplification/overexpression of human epidermal growth factor receptor 2 (HER2+) [8]. Furthermore, the CD73-adenosine axis plays dual and opposite action on BC proliferation depending on the engagement of different adenosine receptors (AdoR). Two of them, AdoR A_1 or A_{2A}, together with ER and estradiol create a regulatory loop for ERα-dependent transcriptional activity [5]. Estrogen, through stimulation of cellular proliferation and due to its genotoxic metabolites [9], as well as progesterone receptor signaling [10,11] are indicated as critical mediators in mammary gland carcinogenesis. Both ER and PR also seem to have a role in the regulation of the balance between *de novo* FA synthesis and their oxidation (FAO) with differential expression of lipid metabolism-related genes depending on the BC subtype [12,13].

Enhanced FA synthesis is one of the critical metabolic adaptations in cancer and a potent therapeutic target with several clinical-stage trials for BC. It provides FAs for membrane biogenesis for rapidly proliferating cancer cells, enriching cancer cell membranes with saturated (SFAs) and monounsaturated FAs (MUFAs). FAs are also utilized for protein modification and energy production through their oxidation (FAO) into acetyl-CoA. While normal breast tissue can also undergo extensive metabolic rewiring of lipid metabolism, this process can be appropriated by BC oncogenes such as *PIK3CA* or *MYC*. In the most aggressive TNBC (triple negative breast cancer) tumors frequently amplified *MYC* oncogene can drive FAO in addition to glycolysis [13,14]. FAO can sustain the viability of the hyperproliferative tumor cells during nutrient deprivation. Under hypoxia, tumor cells can also increase the uptake of extracellular FAs, including dietary PUFAs, needed to generate important mediators or substrates in regulating tissue inflammation [15,16]. Adipocytes, prevalent in the breast stroma can also supply BC with FAs and their continuous interactions facilitate oncogenic-driven metabolic reprogramming of cancer cells [13,14]. CD73 is highly expressed in adipocytes, its expression and activity can be upregulated by docosahexaenoic acid (DHA) [17], and it was shown to stimulate FA esterification increasing lipid synthesis in rat adipocytes [18]. CD73 KO also induced dyslipidemia in a mouse model [19]. However, the role of CD73 in regulating lipid metabolism and its effect on the process of mammary gland tumorigenesis has not been analyzed.

To analyze CD73's role in BC tumorigenesis, we applied a carcinogen/promoter-induced multistage BC model reflecting the developmental pathway of human disease, giving rise to mammary gland tumors with a comparable heterogeneity to the human BCs [20]. We assessed the changes induced by CD73 KO on the development of mammary gland tumors (MGTs) through modulation of lipid metabolism at the transcriptome, proteome, and lipidome levels. The main changes observed were correlated with the data from human tissues and cell lines.

2. MATERIAL AND METHODS

2.1. Murine model of mammary tumorigenesis

All experimental procedures were approved by the Local Ethics Committee and performed per the ARRIVE ethical guidelines [21] and EU Directive 2010/63/EU. Wild-type (WT) (Charles River, Calco, Italy) and CD73 KO C57BL/6 mice [22] were bred and maintained at the Tri-City Academic Experimental Animal Centre of the Medical University of Gdansk (Poland). Mice were housed in individually ventilated cages (23 ± 1 °C, 40 ± 10% humidity) in a light/dark cycle of 12 h/12 h with unlimited access to water and a standard chow diet. Mice were euthanized through cervical dislocation under anesthesia with ketamine and xylazine injected intraperitoneally at 100 mg/kg and 10 mg/kg body weight, respectively.

To induce mammary tumors female WT (n = 43) and CD73 KO (n = 46) C57BL/6 mice were first primed with subcutaneous injection of 15 mg/kg of MPA (medroxyprogesterone acetate, Depo-Provera, Pfizer) at postnatal day (PND) 42.1 mg of DMBA (7,12-dimethylbenz [a]anthracene, #D3254, Sigma–Aldrich) in 0.1 ml of sesame oil was administered by oral gavage on PND 49, 56, 63, 70. After the last DMBA dose, tumor development was monitored by palpation once per week. The overall health of mice was monitored three times a week. On PND 98 randomly chosen WT (n = 4) and CD73 KO mice (n = 5) were euthanized and their right fourth mammary glands were isolated. All mammary glands of these mice were analyzed under the stereoscopic microscope and the lack of developing tumors confirmed it as a potential initiation stage of tumorigenesis. For the other WT (n = 39) and CD73 KO (n = 41) mice, incidence (number of mice with tumors), latency (time from the last DMBA dose to the development of the first palpable tumor), and multiplicity (number of tumors per mouse) were recorded. Mice were euthanized when the tumor reached 10 mm in diameter as measured with a caliper or at PND 273. No mice needed to be euthanized before these end-points due to the loss of more than 10% of the total weight or other reasons.

2.2. Histochemical and immunohistochemical evaluation of murine tumors

MGTs were fixed for 24 h in 4% formalin and processed in a tissue processor (Leica TP-1020). Paraffin-embedded tissue samples were stained with hematoxylin and eosin. Tumor slides were examined using Nikon's Eclipse E600 light microscope (Nikon Instruments Inc., Japan). Photographs were taken with a digital camera (Nikon, DS-Fi1, Nikon Instruments Inc., Japan) and image analysis software (NIS-Elements BR-2.20, Czech Republic). Morphological analysis was done by a pathologist blinded to the experimental protocol. Histopathological evaluation was performed according to the classification by Cardiff et al. [23]. In the case of a heterogeneous mammary gland tumor, the dominant histological type was decisive.

5 μm tissue sections of paraffin-embedded formalin-fixed tumor samples were attached to SUPERFROST®PLUS basic slides (#J1800AMNZ, Thermo Fisher Scientific). After deparaffinization and rehydration, endogenous peroxidase activity was quenched with a peroxidase suppressor for 10 min. Heat-induced antigen retrieval in a water bath for 30 min was performed using 10 mM sodium citrate buffer (pH 6.0) to expose HER2 and progesterone proteins, and EDTA buffer (pH 8.0) to expose estrogen proteins. Following antigen retrieval, tissues were permeabilized in 3% BSA-PBS solution for 30 min at room temperature. Sections were then probed with primary monoclonal antibodies for 1 h at room temperature in a humidified chamber. Mouse anti-mouse anti-ErbB2/HER2 antibody [3B5] (ab16901, dilution 1:500), rabbit anti-mouse anti-Estrogen Receptor alpha antibody [E115] (ab32063, dilution 1:200) were purchased from Abcam (Cambridge, UK). Mouse anti-mouse anti-Progesterone Receptor antibody (PR-AT 4.14) (#MA1-410; dilution 1:500) was purchased from Thermo Fisher Scientific. TBS (Tris-buffered saline) was used instead of the primary antibody for the negative control, and human breast carcinoma was used as a positive control for primary antibodies. Sections were then washed in PBST (0.1% Tween 20 in PBS solution) and the IHC reaction was carried out by an indirect method using an UltraVision Quanto Detection System (#TL-060-QHD, Thermo Fisher Scientific) with 3,3′-diaminobenzidine (DAB) as the chromogen substrate. Tissues were counterstained with hematoxylin and prepared for mounting. The analyses of mounted slides were performed by an experienced pathologist.

IHC reaction for ER, PR, and HER2 was scored by a combination of intensity (0, no reaction; 1, weak reaction; 2, moderate reaction; 3, strong reaction) and proportion (0, $<$5% of positive cells; 1, 5—25% positive cells; 2, 26—50% positive cells; 3, 51—75% positive cells; 4, more than 76% positive cells) scores. A modified Allred scoring system was used, where the final score was derived from the sum of the proportion score (range, 0 to 4) and intensity score (range, 0 to 3). If the total score was $>$4, immunoreactivity was defined as ER/PR/HER2-positive. If the total score was $\leq$4, the sample was designated ER/PR/HER2-negative. ER/PR/HER2 status was scored for positivity in three random fields ($\times$ 400 magnification) and the total percent score was obtained. Then, the median values of ER/PR/HER2 were chosen as cut-offs for high or low immunoreactivity. An experienced pathologist assessed the cellular location and intensity of immunoreactivity in each tissue section. At the same time, a second observer determined whether there were any discrepancies.

2.3. RNA sequencing and differential gene expression analysis of murine samples

To identify differentially expressed genes (DEGs), RNA-seq was performed. Total RNA was extracted from all isolated right fourth mammary glands (MGs) obtained on PND 98 and primary MGTs by using the RNeasy Lipid Tissue Mini Kit (#74804, QIAGEN Sciences) with on-column DNase digestion (QIAGEN Sciences) per the manufacturer's protocol. The concentration and purity of the extracted RNA were determined by using a Qubit 4 Fluorometer and Qubit RNA High Sensitivity Assay Kit (#Q10210, Thermo Scientific). The assessment of the quality of the samples and RNA-seq was performed by Macrogen Europe B.V. (Amsterdam, Netherlands). Libraries were sequenced in a paired-end (2 $\times$ 150 bp) manner on NovaSeq 6000 (True Seq mRNA stranded for poly-A selection) Illumina platform (San Diego, CA, USA) with an average of 40 million total reads per sample.

The libraries have been deposited in the Sequence Read Archive (SRA) database under the PRJNA933922 accession number (www.ncbi.nlm.nih.gov/sra). Analysis was conducted using R statistical software version 4.x.x [24]. The raw reads were first quality-checked and filtered using FastQC [25] and Trimmomatic [26] to obtain high-quality reads. The reads were mapped to the *Mus musculus* reference genome (GRCm39) using STAR [27], counted with featureCounts 2.0.346 [28], and differential gene expression analysis was conducted using DESeq2 1.34.0.47 [29]. The absolute value of fold change $\geq$1.5 and Benjamini-Hochberg adjusted for false discovery rates (FDR) p-value $<$0.05 were used as a criterion to identify differentially expressed genes.

Gene ontology enrichment analysis was performed using the topGO [30] R package. Gene names were mapped to GO terms using the org.Mm.eg.db package [31]. Only GO terms with a p-value $\leq$0.05 were considered significantly enriched. A protein—protein interaction (PPI) network of proteins encoded by DEGs was visualized using the STRING database (string-db.org) [32]. The lines represent text-mining evidence in the PPI network, and their thickness indicates the strength of data support. The bubble colors represent gene involvement in certain GO terms and KEGG pathways.

2.4. Fatty acid profile analysis

The extraction of total lipids from tissue samples was performed according to the method of Folch et al. [33]. After lipid hydrolysis with KOH in methanol, washing with water/n-hexane, the n-hexane phase was evaporated to dryness under a stream of nitrogen. Nonesterfied FAs were then methylated with 10% boron trifluoride. The FA methyl esters (FAMEs) were analyzed with GC-EI-MS QP-2010 SE (Shimadzu, Japan), as described by Mika et al. [34]. Heatmaps of the unsupervised hierarchical clustering of the FA data were generated with the GenePattern platform [35] using Pearson correlation. It represents the fold changes between the means of the percentages of fatty acids measured by mass spectrometry, red denotes up-regulation, and blue down-regulation. Row normalization was used, and the data from each animal was reordered based on the correlations according to the dendrogram on the top. Clusters go from the root at the left to the leaf node for each fatty acid. The branch shows the similarity, the more similar the shorter the branch.

2.5. *In silico* analysis of publicly available patient datasets

Differential gene expression analysis of mRNA expression data was performed in 168 non-malignant breast tissue samples from the Genotype-Tissue Expression (GTEx) project (accessed from Human Protein Atlas database, https://www.proteinatlas.org/) and 1904 malignant breast tissue samples from the METABRIC cohort (accessed from cBioPortal for Cancer Genomics, https://www.cbioportal.org/). Samples were classified by trichotomization of *NT5E* gene expression (CD73 high — T1, CD73 low — T3). In the METABRIC cohort, only double-positive (ER+/PR+) and double-negative (ER-/PR-) cases were included in further analysis. DEGs were identified based on the following criteria: FDR$<$0.05 and |log2FC|$>$1. GO and KEGG pathways enrichment

analyses were conducted using the Functional Annotation Tool by DAVID Bioinformatics Resources 6.8 [36] and visualized using R.

Copy number aberrations, Copy number variants, and Single nucleotide polymorphism data from the METABRIC cohort were retrieved from cBioPortal for Cancer Genomics (https://www.cbioportal.org/), while IntClust Status, TMB Score, GII, CAAI, and Number of breakpoints were obtained from [37].

scRNA-seq datasets covering *NT5E*/*Nt5e*, *PPARG*/*Pparg*, and lipid-metabolism-related gene expression, as well as cell population distribution in murine and human white adipose tissue [38] and in human healthy breasts [39] were analyzed and visualized using software from Single Cell Portal (https://singlecell.broadinstitute.org/). Bubble plots of mean expression of *NT5E*/*Nt5e* and *PPARG*/*Pparg* for cell subsets were generated with Single Cell Portal software and unsupervised-hierarchical clustering heatmap of *NT5E*, *PPARG*, and lipid-metabolism related DEGs mean expression was generated with the GenePattern platform. For clustering only selected DEGs correlating with NT5E with Spearman R correlation coefficient rho $\leq$ |0.500| were taken into study.

mRNA expression data from 48 breast cancer cell lines from the CCLE database (https://depmap.org/) was analyzed and heatmaps of selected genes were generated using GraphPad Prism 9 software.

2.6. Patients and tissue specimens

This retrospective study reviewed the medical data of 135 BC patients treated between 2001 and 2008 at the Medical University of Gdansk and Regional Cancer Centre in Bydgoszcz, Poland [40]. Inclusion criteria were stage I-III BC and signed informed consent. The majority of patients (91%) underwent primary surgery followed by systemic treatment, radiotherapy, or both. Nine percent of patients were administered induction chemotherapy. Tumor samples were collected by surgical excision or excisional biopsy before any systemic treatment and were formalin-fixed paraffin-embedded according to standard procedure. Table S1 shows the characteristics of patients included in this study.

2.7. Immunohistochemistry (IHC)

5 μm tissue sections of FFPE murine tumor samples or 3 μm tissue sections of FFPE human TMA (for PPARγ), were deparaffinized and rehydrated, then endogenous peroxidase activity was quenched with a peroxidase suppressor for 10 min. Heat-induced antigen retrieval for 10 min was performed using 10 mM sodium citrate buffer (pH 6.0, 65 °C) to expose targeted proteins. Following antigen retrieval, tissues were permeabilized in 1% PBST (0.1% Tween 20 in PBS solution) solution for 5 min at room temperature. Sections were then blocked with either 2.5% Normal Goat Serum Blocking Solution (#S-1012-50, Vector Laboratories) for 20 min or M.O.M® Mouse IgG Blocking Reagent (#MKB-2213-1, Vector Laboratories) for 30 min followed by M.O.M® 2.5% Normal Horse Serum (#MP-7451, Vector Laboratories) for 20 min. After that sections were incubated with primary antibodies: rabbit anti-PPARγ (#A11183; dilution 1:400, Abclonal), rabbit anti-phospho-AMPKα1/2 (#AP1441, 1:300, Abclonal), mouse anti-MLH1 (#A20544, 1:300, Abclonal), rabbit anti-γ-H2A.X (#A9718, 1:400, Cell Signaling) for 2 h at room temperature in a humidified chamber. PBST was used instead of the primary antibody for the negative control, and human breast carcinoma was used as a positive control for primary antibodies. Sections were then washed in PBST and the IHC reaction was carried out by an indirect method using ImmPRESS® HRP Goat Anti-Rabbit IgG Polymer Detection Kit, Peroxidase (#MP-7451, Vector Laboratories) (PPARγ), M.O.M® ImmPRESS® Horse Anti-Mouse IgG Polymer Reagent, Peroxidase (#MP-2400, Vector Laboratories) (MLH1) or goat anti-rabbit*HRP (#A9169, Sigma Aldrich) (phospho-AMPKα1/2, γ-H2A.X) with NovaRed® (#SK-4800, Vector Laboratories) as the chromogen substrate. Tissues were counter-stained with hematoxylin and prepared for mounting. Slides were scanned at 20× magnification by VS200 ASW microscope (Olympus Corp., Japan). The analyses of mounted slides were performed by two independent observers.

IHC reaction was scored (Staining Score) by multiplying intensity (0, no reaction; 1, weak reaction; 2, moderate reaction; 3, strong reaction, 4, very strong reaction) and stained area (% of positively stained cells in total tumor cells) scores. Signals were measured independently, both from nucleus and cytoplasm of cells. PPARγ pathway activation is measured as a ratio of nucleus to cytoplasm expression of PPARγ in tumor cells.

2.8. Human and murine cell lines

4T1 (#CRL-2539), BT-474 (#HTB-20), BT-549 (#HTB-122), CAMA1 (#HTB-21), HCC1143 (#CRL-2321), HCC1428 (#CRL-2327), HCC1806 (#CRL-2335), HCC1937 (#CRL-2336), HCC70 (#CRL-2315), Hs578t (#HTB-126), MCF7 (#HTB-22), MDA-MB-231 (#HTB-26), MDA-MB-361 (#HTB-27), MDAMB-436 (#HTB-130), MDA-MB-453 (HTB-131), SK-BR-3 (#HTB-30), T47D (#HTB-133) and ZR-75-1 (#CRL-1500) were acquired from the American Type Culture Collection (ATCC, Manassas, USA). CAL51 (#ACC302) was acquired from the Leibniz Institute DSMZ-German Collection of Microorganisms and Cell Cultures (DSMZ, Braunschweig, Germany). E0771 (#CRL-3461) was a kind gift from Andreas Möller (QIMR Berghofer Medical Research Institute, Herston, Queensland, Australia).

Cell lines were routinely cultured either in DMEM (#10-013-CV, Corning) (E0771, Hs578t, MCF7, MDA-MB-231, MDA-MB-361, SK-BR-3, T47D), MEM (#10-010-CV, Corning) (CAMA1) or RPMI-1640 (#10-040-CV, Corning) (4T1, BT-474, BT-549, CAL51, HCC1143, HCC1428, HCC1806, HCC1937, HCC70, MDAMB-436, MDA-MB-453, ZR-75-1) supplemented with 10% fetal bovine serum (FBS, #BWSTS181F, VWR) and 1% of penicillin/streptomycin (#P7539, Sigma—Aldrich). For selected cell lines culture medium was supplemented with 5 μg/ml (BT-474) or 10 μg/ml (Hs578t, MDA-MB-436) human insulin (#I9278, Sigma—Aldrich) or 1% of sodium pyruvate (#S8636, Sigma—Aldrich) (4T1, E0771). All cells were maintained in 5% CO_2 at 37 °C. All cells were regularly tested for mycoplasma contamination and cultured at low passages to avoid genome drift.

2.9. Western blot analysis of cell lysates

Cells were grown to 70—80% confluence, stimulated with 200 μM AOPCP (Adenosine 5′-α,β-methylene diphosphate - CD73 inhibitor) (#M3763, Sigma—Aldrich) for 8h, 24h and 48h, scraped and lysed with RIPA Buffer (#89901, Thermo Scientific) supplemented with cOmplete™ Protease Inhibitor Cocktail (#04693116001, Roche) on ice. Protein concentration was quantitated and determined using the Pierce™ BCA Protein Assay Kit (#23225, Thermo Scientific). An equal amount of protein (~15 μg) per lane was loaded and separated by SDS-PAGE. Proteins were then transferred onto PVDF membranes (#3010040001, Sigma—Aldrich), blocked in skimmed milk in TBS-T, and immunoblotted overnight with specific primary antibodies at 4 °C. Primary antibodies used for the experiments were as follows: GSTA3 (#A17491, 1:500) and MLH1 (#A20544, 1:250), PPARγ (#A11183, 1:2000) purchased from Abclonal; γ-H2A.X (#A9718, 1:500) purchased from Cell Signaling; GPx-1/2 (#sc-133160, 1:1000) and SOD1 (#sc-101523, 1:500) purchased from SantaCruz Biotech; β-actin (#A5441, 1:4000), CD73 (#ZRB1035, 1:500) and GAPDH (#ABS16, 1:4000) purchased from Sigma—Aldrich. Appropriate secondary

antibodies conjugated with AlexaFluor®790 or AlexaFluor®680 (#715-655-150, #111-625-144, Jackson ImmunoResearch) and Odyssey system (LI-Cor, Lincoln, USA) were used for the visualization of detected proteins. Densitometry of bands representing detected proteins was done with ImageJ software. Relative expression of proteins was counted as a percent of a geometric mean of β-actin and GAPDH level of expression. For each cell line separately, bar plots were generated based on densitometry results from at least 3 repetitions per condition. For summarized graphs, results for a group of cell lines were presented as normalized data from three independent pairs of repetitions (Control vs AOPCP, 48h) from each cell line.

2.10. Glutathione S-transferase activity assay

The assay was performed according to the protocol of the Glutathione S-transferase (GST) Assay Kit (#CS0410, Sigma Aldrich). Briefly, $1{,}5 \times 10^5$ of cells of selected cell lines (4T1, BT-474, CAL51, E0771, HCC1143, HCC1806, MCF7, MDA-MB-231, MDAMB-436, T47D) were seeded to 24 well plates for overnight to attached, then stimulated with 200 μM AOPCP for 48h. Cells were next washed with PBS and solved in 200 μl Lysis Buffer (0.5% Triton X-100 in 0.1M PBS pH = 7,2) on ice for 15 min. After that, lysates were collected, and centrifugated at 14000G for 10 min at 4 °C. 20 μl of supernatants were placed into 96-well plates, 180 μl of Substrate Solution was added to each sample well, and GST positive control and Blank were placed into the plate. The absorbance of samples, blank, and positive control was measured every minute in 8-time points in the plate reader (Synergy H1, BioTek) at 340 nm. Calculation of results was performed according to protocol and GST activity was stated in μmol/ml/min. All analyses include results from at least 4 biological repetitions per condition for each cell line, presented for each cell line separately. For summarized graphs, results for a group of cell lines were presented as normalized data from four independent pairs of repetitions (Control vs AOPCP, 48h) from each cell line and compared to Control PR+.

2.11. Quantification of ROS level by flow cytometry analysis

$1{,}5 \times 10^5$ of cells of selected cell lines (BT-474, CAL51, E0771, HCC1143, HCC1806, MCF7, MDA-MB-231, MDAMB-436, T47D) were seeded to 24 well plates for overnight to attached, then stimulated with 200 μM AOPCP for 48h. Then control cells were incubated with 20 mM H_2O_2 (#216763, Sigma Aldrich) for 30 min or 20 mM N-acetyl-L-Cysteine (NAC, # A15409.36, Thermo Fisher Scientific) for 15 min, after that 20 μM carboxy-H_2-DCFDA (#C400, Thermo Fisher Scientific) was added to the medium of all cells and cells were incubated for 30 min in 37 °C. Cells were then washed with PBS and detached with Trypsin solution (#25-053-CI, Corning). After washing cells were resuspended in 200 μl of PBS. Cells were subjected to cytometric analysis (CytoFLEX, Beckman Coulter) at λex = 488 nm, λem = 525/40 nm. All measurements were carried out with 1×10^4 cells that exhibited the typical forward and side scatter of non-disintegrated cells. All analyses include three technical measurements for each biological repeat, from at least 3 biological repetitions per condition for each cell line, presented for each cell line separately. For summarized graphs, results for a group of cell lines were presented as normalized data from three independent pairs of repetitions (Control vs AOPCP, 48h) from each cell line and compared to Control PR+.

2.12. Statistical analyses

Mean values were obtained from at least three separate experiments and reported as the mean (±SEM). Statistical analyses were performed with the unpaired t-test or Mann—Whitney test for comparisons of two unpaired groups, paired t-test or Wilcoxon matched-pairs test for comparisons of two paired groups, ANOVA or Kruskal—Wallis test for comparisons of more than two groups, the two-sided Chi-square test or Fisher test for binomial decomposition, and the logRank test for survival analyses and Kaplan—Meier curves. Statistical analyses were performed with Statistica 13 and GraphPad Prism 9 software. A p-value <0.05 was considered statistically significant.

3. RESULTS

3.1. CD73 KO delays the onset of hormone receptor-negative MGTs in a carcinogen-induced mouse model

To assess the effect of CD73 depletion on mammary gland tumorigenesis, we induced the development of MGTs in WT and CD73 KO mice with C57BL/6 genetic background using a two-stage chemical tumorigenesis protocol (Figure 1A). Histopathological analysis classified MGTs as mostly (over 64%) adenocarcinomas: papillary, solid, glandular, or acinar (Fig. S1) and CD73 KO did not modify their ratio (Table S2). There was no significant difference between WT and CD73 KO groups in the incidence of MGTs (72% and 76% of mice with tumors, respectively) but CD73 KO was associated with significantly longer tumor-free survival (TFS) after tumor induction (Figure 1B).

Most of the MGTs were hormone receptor-positive (HR+), expressing either progesterone and/or estrogen receptors (Fig. S2), with no significant difference in the distribution of PR, ER, and HER2 between CD73 KO and WT groups at the protein (Figure 1C) and mRNA level (Fig. S3). The CD73 KO-induced increase in TFS was significant in an HR-negative (HR-), but not in an HR-positive (HR+) group, with a similar effect when mice were stratified only according to PR or ER expression (Figure 1D). While CD73 KO-induced effect on TFS was also present in TNBC group, HER2 overexpression did not affect TFS in CD73 KO mice (Figure 1E). However, this study was limited by the low incidence of HER2 tumors (Figure 1C). Furthermore, analysis of the correlation between CD73 and ER expression was limited by a high fraction of negative results for ER protein expression, confirmed with RNA-seq results (Fig. S3). It is consistent with the model applied, using MPA, a synthetic analog of progesterone for priming before induction with a cancerogene (DMBA), and a long time that is needed for tumor development and growth. It is concurrent with the reduced expression of the ERα isoform in older mice that were subjected to high levels of progesterone through pregnancy [41]. Nevertheless, as the quantitative PR load correlates with the quantitative ER load [42] and BC ER-low cases are associated with higher PR expression [43], we were able to correlate results with PR expression.

The analysis of RNA-sequencing data from MGs isolated from mice at PND 98, four weeks after the last DMBA dose, identified 336 DEGs (FDR <0.05) between WT and CD73 KO MGs. Gene Ontology (GO) functional annotation analysis of upregulated and significantly enriched DEGs showed that (1) the biological processes were mainly involved in the regulation of cell motility, cell—cell interactions, and lipid metabolism, especially FA biosynthesis and β-oxidation; (2) the cell components involved were mainly integral components of membranes, cell-cell junctions, and peroxisomes (Figure 1F). Changes in the FA metabolism were confirmed by mass spectrometry analysis of the FA profile of mammary glands from the initiation stage (Table S3). The heat map of the unsupervised-hierarchical clustering of the data shows increased percentages of saturated long-chain FAs, myristic (14:0) and palmitic (16:0) in the CD73 KO group (Figure 1G). It is consistent with an increased expression of genes involved in the metabolism of acetyl-coenzyme A (acetyl-CoA) (e.g., *Aacs, Acly, Acaca, Acat2*) (Figure 1F,H) (Table S4), an intracellular carbon source for FA biosynthesis, as well as genes involved in the elongation of saturated and mono-unsaturated FAs

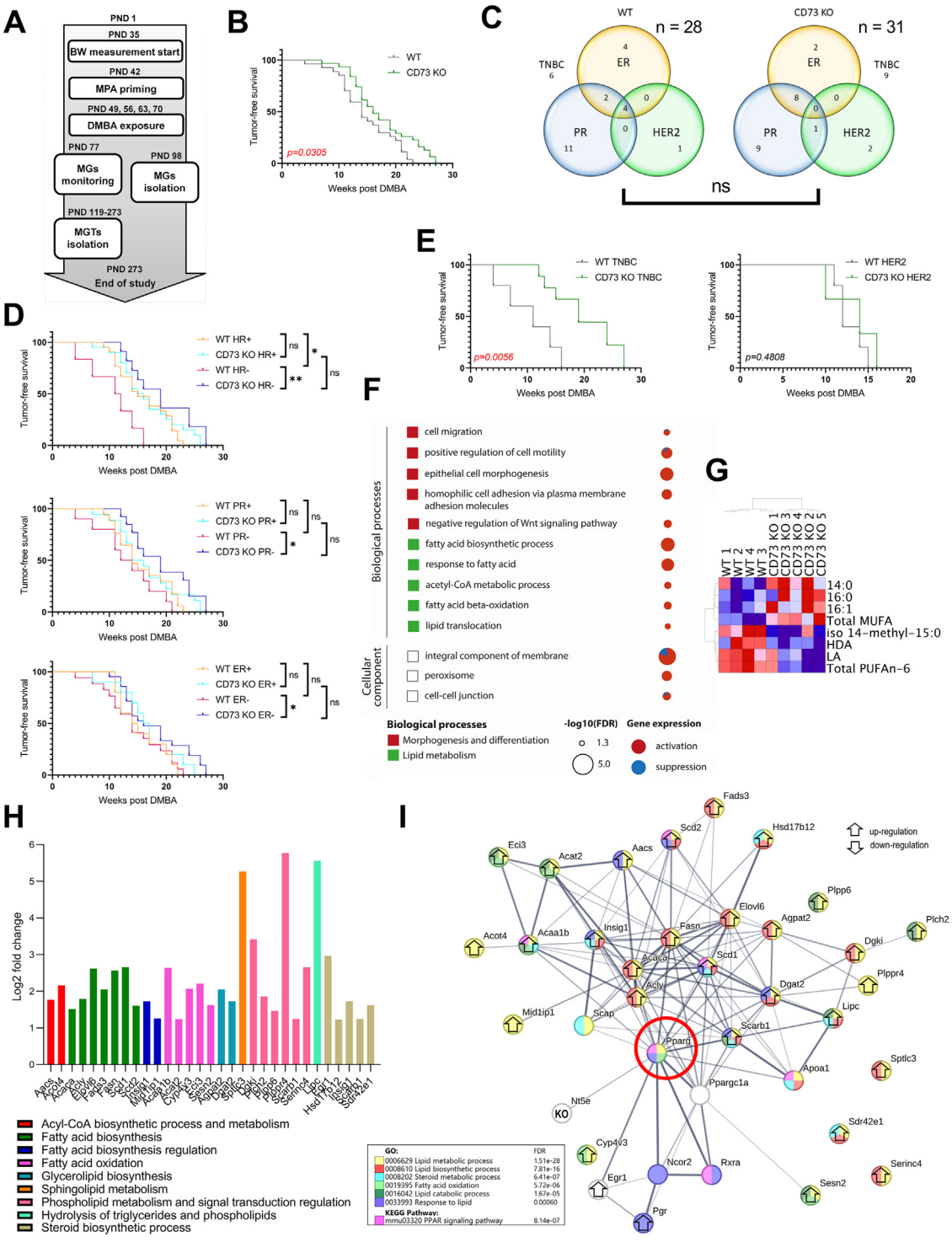

Figure 1: Effect of CD73 KO on MPA/DMBA-induced mammary gland tumorigenesis. (A) Design of the study. (B) Kaplan–Meier curve for the tumor-free survival from the last DMBA dose to the development of a first palpable mammary gland tumor (logRank test values are shown) (WT, n = 28, CD73 KO, n = 31). (C) Distribution of BC molecular markers in WT and CD73 KO mice groups. (D) Kaplan–Meier curves for tumor-free survival in WT and CD73 mice grouped according to IHC staining for hormone receptors (HR), estrogen, or progesterone (logRank test values are shown). *p < 0.050, **p < 0.010, ***p < 0.001. (E) Kaplan–Meier curves for tumor-free survival in TNBC and HER2+ groups in WT and CD73 mice (logRank test values are shown). (F) The bubble matrix represents enrichment results of pathways changed by CD73 KO in mammary glands at the initiation stage of MG tumorigenesis compared to WT mice. The matrix illustrates the -log10(FDR) values and percentage of up- (red) or down-regulated (blue) genes mapped to each term (pie chart). (G) The heatmap of the unsupervised hierarchical clustering of the differences between WT and CD73 KO mice in the fatty acids profile of mammary glands at the initiation stage of tumorigenesis (PND 98, 4 weeks after the last DMBA dose, WT, n = 4; CD73 KO, n = 5). (H) Lipid-metabolism-associated DEGs significantly changed by CD73 KO identified in mammary glands at the initiation stage of mammary gland tumorigenesis. (I) Visualization of a protein–protein interactions network of products of genes involved in FA metabolism in correlation with *Pgr* generated using the STRING database. CD73 KO-induced changes in gene expression are denoted with arrows..

with 12, 14, and 16 carbons (*Elovl6*) [44]. An increase in total monounsaturated FAs (total MUFA), especially palmitoleic acid (16:1) indicates an increased FA desaturation consistent with an up-regulation of *Scd1* desaturase, that mainly catalyzes the addition of double bond to palmitic acid (16:0 -> 16:1) and stearic acid (18:0 -> 18:1). On the other hand, a significant decrease in the percentage of total PUFAn6, mainly hexadecadienoic acid (16:2n-6; HDA) and a dietary essential FA and a primary PUFAn6 - linoleic acid (C18:2n-6; LA), corresponds with an up-regulation of FA β-oxidation indicated by GO enrichment analysis (Figure 1F). It is supported by a decrease in the body weight of CD73 KO mice at the initiation stage of MG tumorigenesis (Fig. S4A).

GO enrichment analysis also indicates CD73 depletion-induced transcriptomic changes in epithelial cell morphogenesis (Figure 1F), a process in mammary gland development highly regulated by progesterone and estrogen receptors [45]. At the initiation stage of tumorigenesis, mRNA expression of the gene coding for progesterone receptor (*Pgr*) in mammary glands of CD73 KO mice relative to WT was significantly higher (log2 fold change of 3.52, p-value adjusted for false discovery rates = 0.016). There was no difference in mRNA expression of genes coding for estrogen receptor (*Esr1*) and HER2 (*Erbb2*). Protein—protein interaction (PPI) network generated for the products of identified DEGs using the STRING database indicates a tight interplay between the expression of the genes involved in FA metabolism and *Pgr*, which were all consistently upregulated in the CD73 KO group (Figure 1I). It also highlights PPARγ (peroxisome proliferator-activated receptor gamma), a transcription factor regulating an expression of genes involved in lipid metabolism, as an important connective node right in the middle of the network.

3.2. CD73 regulates lipid metabolism in hormone-sensing epithelial cells

Analysis of the publicly available GTEX transcriptomic data of mammary glands from healthy women also shows upregulation of genes involved in lipid metabolism in MGs with low compared to high expression of the CD73 gene (*NT5E*) (Figure 2A). The affected processes included lipid storage and its regulation, triglyceride biosynthesis and catabolic process, cholesterol metabolism, and lipid catabolism, but also regulation of progesterone secretion. KEGG analysis highlighted the upregulated expression of DEGs associated with the regulation of lipolysis in adipocytes and fatty acid biosynthesis, with an enrichment of PPAR, AMPK, and adipocytokine signaling pathways.

To indicate the cell population in a mammary gland most involved in the CD73 KO-induced changes we used single-cell RNA-sequencing (scRNA-seq) data from Broad Institute datasets. In white adipose tissue (WAT) of human and murine healthy mammary glands [38], there is no significant correlation between *PPARG/Pparg* and *NT5E/Nt5e* expression, in general, and for specific subpopulations of cells including adipocytes and their progenitor/stem cells (ASPCs), vascular cells, and immune cells (Figure 2B). In both species adipocytes and pericytes have the highest *PPARG/Pparg* expression, while there are some differences in *NT5E/Nt5e* expression, especially in ASPCs, LEC (lymphatic endothelial cells) and neutrophil subpopulations. Next, we analyzed scRNA-seq data from a human breast atlas [39]. There is a significant correlation between *NT5E* and *PPARG* expression (Spearman R rho = 0.753) for a population consisting of epithelial cell subsets, alveolar cells (AV), hormone sensing cells (HS), and basal cells (BA) as well as endothelial cells, fibroblasts, and immune cells. The unsupervised-hierarchical clustering of Spearman R correlation matrix between *NT5E* expression and selected lipid-metabolism-associated genes (Figure 2C), indicates a strong correlation between low CD73 expression and high expression of genes involved in the metabolism of acetyl-coenzyme A (acetyl-CoA) (*Aacs, Acaca*) in the subpopulation of hormone-sensing cells. Similarly, as in MGs from CD73 KO mice at the initiation stage of tumorigenesis.

3.3. CD73 regulates FA metabolism during BC development

We explored RNA-seq data from MGs and MGTs to analyze CD73's role in the development of a primary tumor in a mammary gland (Figure 3A). About 17% of DEGs between the initiation and progression stages were unique for the CD73 KO or WT group indicating CD73-induced differences in the gene expression during tumor development. GO enrichment analysis suggests that CD73 KO at the progression stage suppresses fat cell differentiation together with the lipid metabolic process, simultaneously nullifying the effect observed at the initiation stage on FA biosynthesis and β-oxidation (Figure 3B). It is accompanied by suppressed regulation of epithelial cell differentiation and mammary gland development, as well as cell—cell signaling, transmembrane transport, and reactive oxygen species metabolic process. Therefore, we compared the FA profiles of MGs and MGTs. In the WT group, the most significant change induced by tumor development was an increase in the total percentage of anteiso branched-chain FAs (total anteiso BCFA), which together with iso BCFAs are indicated to inhibit FA biosynthesis in human BC cells [46] (Figure 3C, Table S5). In the CD73 KO group, besides a similar increase in total anteiso BCFAs, there was a significant increase in the percentage of FAs with longer chains, saturated (18:0, 20:0; 21:0; 22:0; 24:0) and monounsaturated (24:1), a PUFAn3, ETA (eicosatetraenoic acid), and some PUFAn6, especially arachidonic acid (ARA), and its elongation product, adrenic acid (AdA) (Figure 2C, Table S6). There was also a corresponding decrease in the percentage of palmitic acid (16:0) and eicosenoic acid (20:1). As a result, at the progression stage itself, the differences in FA profiles between WT and CD73 KO groups in FA profiles were abolished (Table S7).

Next, we compared the CD73-associated changes in the transcriptome of healthy mammary glands from GTEX datasets and breast carcinomas from patients from the METABRIC cohort (Figure 3D). The GO analysis of significantly enriched DEGs shows a similar nullifying effect of low NT5E expression in BC progression on initiation-induced changes in lipid and FA metabolism in mammary glands, when compared to NT5E high groups (Figure 3E). Comparison of unsupervised hierarchical clustering of genes involved in KEGG pathways (PPARG, AMPK, and adipocytokine signaling pathways, regulation of lipolysis in adipocytes and fatty acid biosynthesis) analyzed by GSEA from GTEX datasets (Figure 2A) with the METABRIC datasets confirms changes induced by BC progression (Figure 3E).

Immunohistochemical staining of murine MGTs for PPARγ showed its significantly higher nuclear localization in the WT group compared to the CD73 KO group indicative of its activation (Figure 3F). We also observed a significant drop in *Pparg* expression at the transcriptomic level in CD73 KO mice (log2 fold change of −1,89, p-value adjusted for false discovery rates = 0.0008). It indicates, that CD73 might regulate lipid and FA metabolism through the PPARγ signaling pathway during tumorigenesis in mammary glands.

3.4. CD73 regulates lipid metabolism, stress response, and mutational tumor burden in association with the development of PR-negative tumors

Next, we analyzed the effect of CD73 expression on nuclear localization and activation of PPARγ in murine MGTs in correlation with their PR status. In PR-negative tumors, PPARγ nuclear localization (Figure 4A) and its activation (Figure 4B) were decreased in the CD73 KO group,

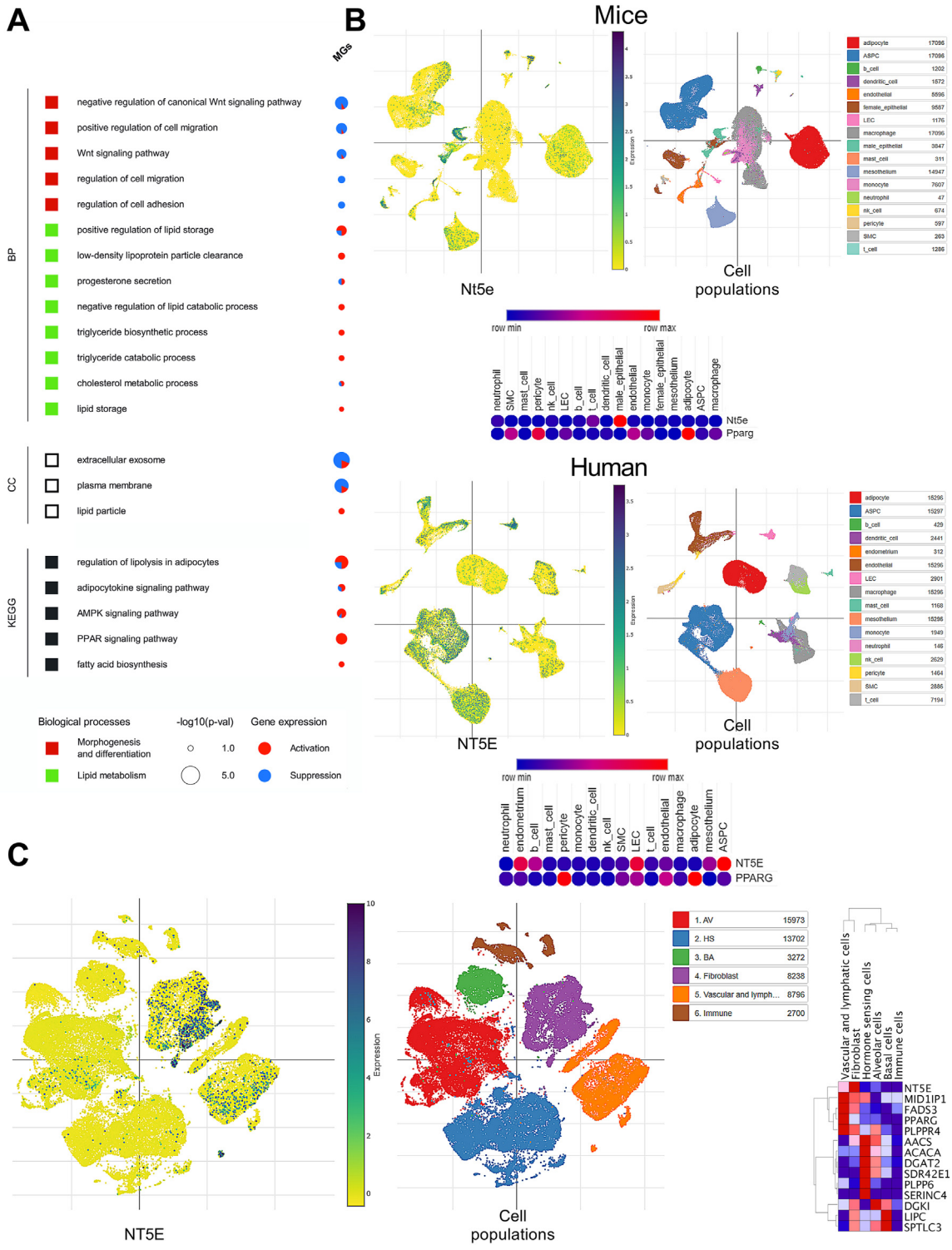

Figure 2: CD73-dependent regulation of lipid metabolism and PPARγ pathway in healthy murine and human mammary glands. (A) The bubble matrix represents GO and KEGG results of pathways associated with *NT5E* gene expression in the GTEX collection of healthy women's breast tissues. The matrix illustrates the -log10 (p-value) and percentage of genes up- or down-regulated (pie chart) in the *NT5E* low group compared to the *NT5E* high group. (B) Expression of *NT5E*/*Nt5e* (CD73) and *PPARG*/*Pparg* (PPARγ) on the single-cell level (scRNA Seq) in murine and human white adipose tissue from mammary glands. Feature plot visualizing gene expression levels of *Nt5e*, UMAP plot with identified cell populations assigned (color key depicted on the graph), and dot plot visualizing gene expression levels of NT5E/*Nt5e* and *PPARG*/*Pparg* in cell subsets. (C) Expression of NT5E and *PPARG* on the single-cell level (scRNA Seq) in human mammary glands. Feature plot visualizing gene expression levels of *NT5E*, UMAP plot with identified cell populations assigned (color key depicted on the graph), and the heatmap of the unsupervised-hierarchical clustering of Spearman R correlation matrix of *NT5E, PPARG,* and other DEGs in cell subsets. DEGs were selected based on the list of lipid-metabolism-associated DEGs significantly changed by CD73 KO identified in mammary glands at the initiation stage of mammary gland tumorigenesis. For clustering, only DEGs correlating with *NT5E* with Spearman R correlation coefficient rho $\leq$ |0.500| were taken into the study..

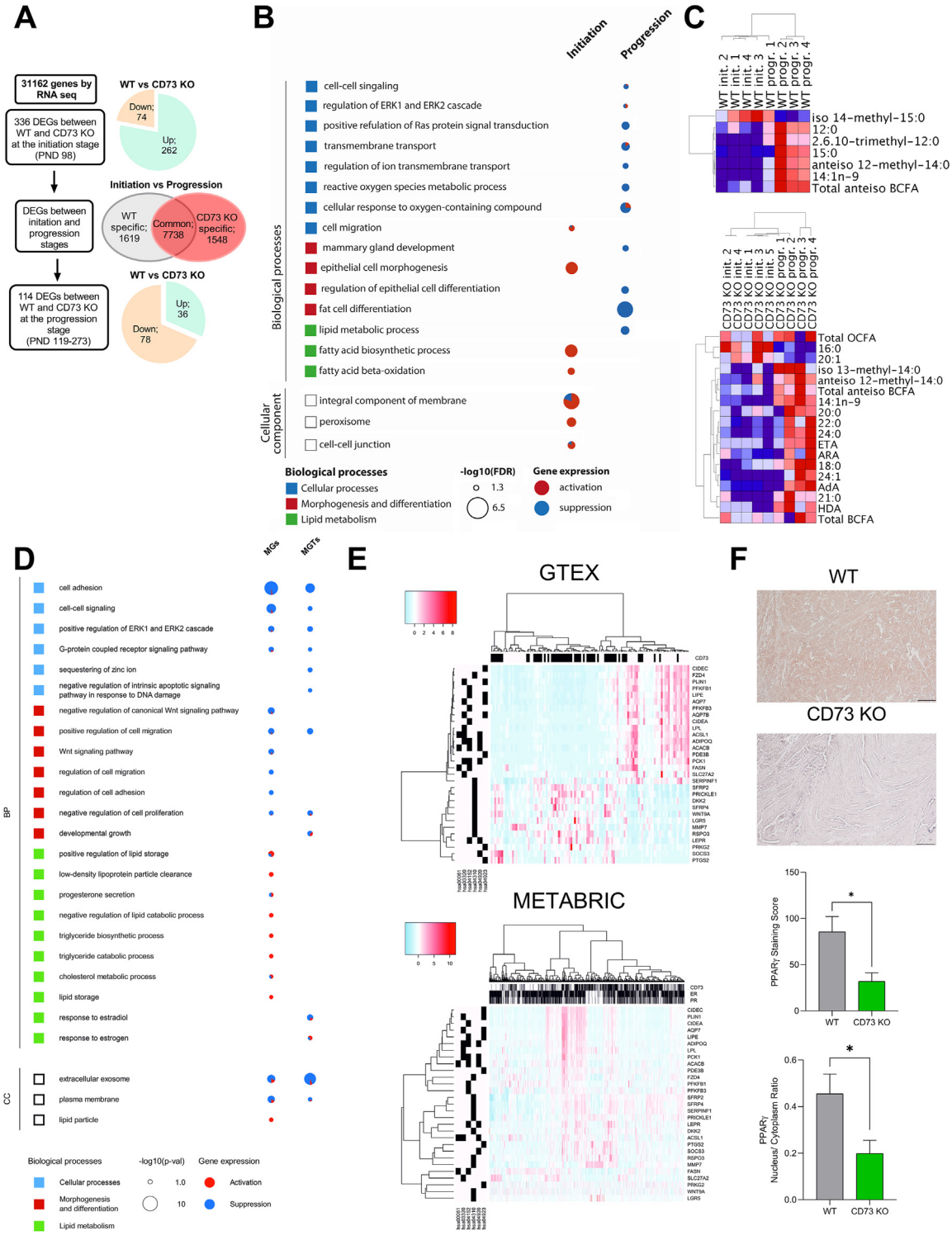

Figure 3: CD73 KO induced changes in FA metabolism at mammary gland tumorigenesis' initiation and progression stage. (A) Flow chart of murine MGTs RNA-seq analysis. (B) The bubble matrix represents enrichment results of CD73 KO-induced changes in mammary glands at the initiation stage and in MGTs at the progression stage. (C) Differences in the FA profile (%) of MGs at the initiation stage (PND 98, 4 weeks after the last DMBA dose) and MGTs from the progression stage (at the experimental end-point) in the WT group (initiation, n = 4; progression n = 4) and the CD73 KO group (initiation, n = 5; progression n = 4) (ratio 1:1 of PR-negative and PR-positive tumors). (D) The bubble matrix represents the enrichment results of pathways associated with *NT5E* gene expression in the GTEX collection of healthy women's breast tissues and breast tumors of METABRIC patients. The matrix illustrates the -log10 (p-value) values and percentage of genes up- or down-regulated (pie chart) in the *NT5E* low group compared to the *NT5E* high group. (E) Heatmap of unsupervised hierarchical clustering of the expression of genes associated with lipid metabolism from the GTEX and the METABRIC datasets with the *NT5E* expression labeled as high (black) or low (white). Genes were selected by FDR<0.05 and |log2FC|>1 criteria. (F) Immunohistochemical staining for PPARγ of MGTs (WT, n = 21; CD73 KO, n = 22). PPARγ Staining Score represents the nuclear localization of PPARγ. PPARγ pathway activation is measured as a ratio of nucleus to cytoplasm expression of PPARγ in tumor cells. Mean + SEM. The scale bar represents 200 μm. Mann–Whitney test, *p < 0.050.

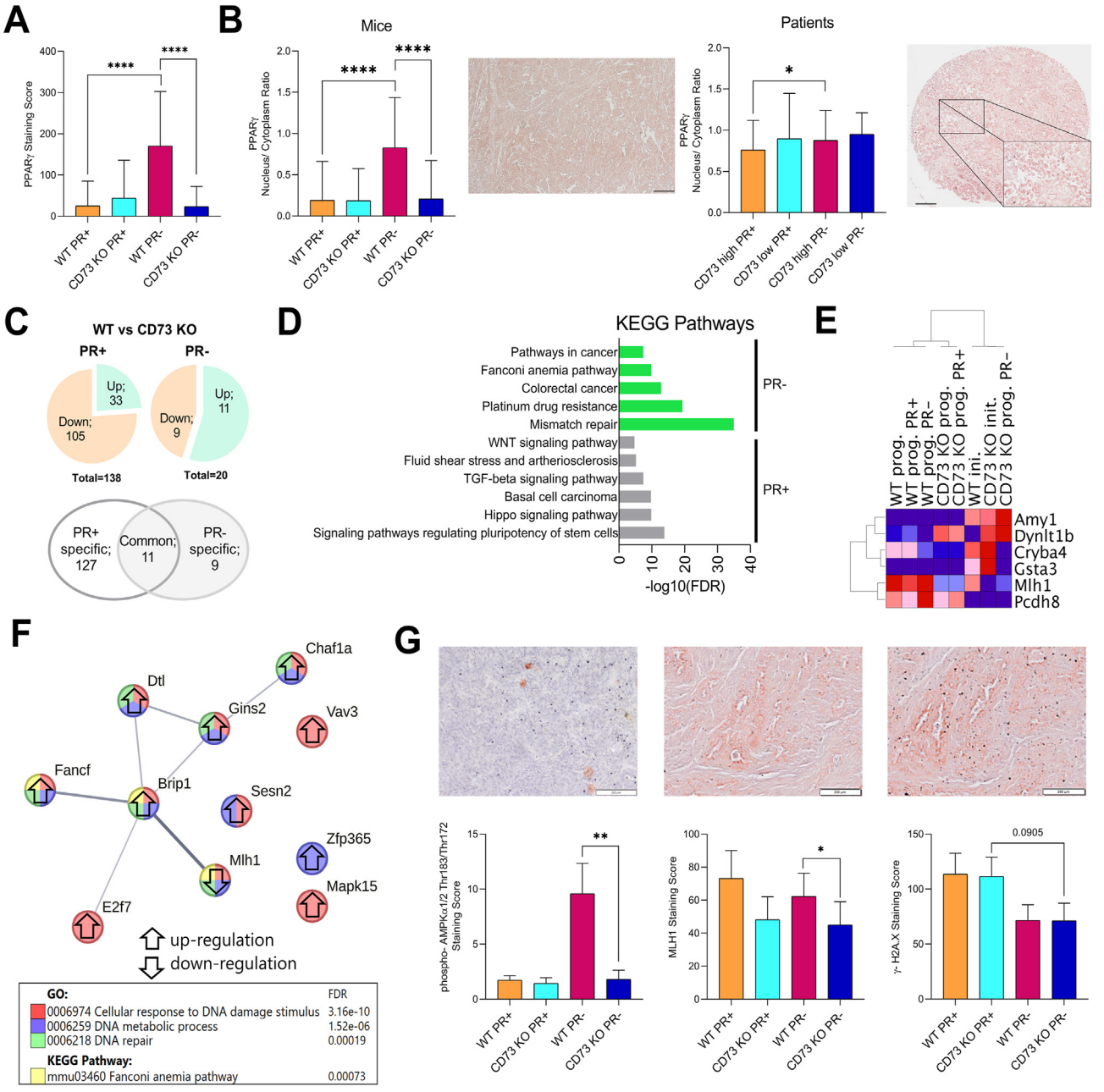

Figure 4: CD73 through PPARγ regulates lipid metabolism and tumor mutational burden in association with PR expression. (A) Immunohistochemical staining for PPARγ of MGTs. PR -negative MGTs (WT, n = 8; CD73 KO, n = 13) and PR-positive MGTs (WT, n = 13; CD73 KO, n = 10). Mean + SEM. The scale bar represents 200 μm. Kruskal–Wallis test. (B) Immunohistochemical staining for PPARγ activation measured as a ratio of nucleus to cytoplasm expression of PPARγ in tumor cells. Mice: PR-negative MGTs (WT, n = 8; CD73 KO, n = 13), PR-positive MGTs (WT, n = 13; CD73 KO, n = 10); Patients: PR-negative BC (CD73 high, n = 37; CD73 low, n = 17) and PR-positive BC (CD73 high, n = 64; CD73 low, n = 16). Mean + SEM. The scale bar represents 200 μm. Kruskal–Wallis test. (C) Flow chart of murine MGTs RNA Seq analysis. (D) CD73 KO-induced changes in KEGG pathways in PR+ and PR- MGTs. (E) The heatmap of the unsupervised hierarchical clustering of DEGs specific for PR-negative tumors according to the stage and PR status. (F) Visualization of a protein–protein interactions network of products of genes from GO:0006974 (cellular response to DNA damage stimulus) pathway at the initiation stage generated using the STRING database. CD73 KO-induced changes in gene expression are denoted with arrows. (G) Immunohistochemical staining for p-AMPKα1/2, MLH1, and γ-H2A.X of MGTs. Mean + SEM. The scale bar represents 200 μm. Kruskal–Wallis test. *p < 0.050, **p < 0.010, ****p < 0.0001.

while in the PR-positive tumors, it was at a comparable low level independently of CD73 expression. It indicates that CD73 can upregulate activation of the PPARγ signaling pathway in PR-negative MGTs. We observed a similar effect for human PR-negative BCs with high expression of CD73 (Figure 4B), even if the sample size of CD73 low tumors limited the study.

To understand the mechanism underlying these changes, we assessed DEGs (FDR <0.05) between WT and CD73 KO MGTs stratified by their PR status (Figure 4C). The growth rate of primary tumors, measured from the moment they were palpable, was not modified by CD73 KO and PR status of MGTs (Fig. S4B), therefore, the changes in gene expression might reflect the pathways modified during an earlier stage

of tumor development. KEGG pathway analysis of 20 DEGs identified for PR-negative MGTs pointed out mismatch repair as one of the most enriched terms (Figure 4D). Unsupervised hierarchical clustering analysis of the protein-coding DEGs unique for PR-negative MGTs, grouped CD73 KO PR-negative tumors with MGs at the initiation stage, both WT and CD73 KO. These genes are involved in mitogenic signaling (*Dynlt1b*, *Pcdh8/PAPC*), stress response (*Mlh1, Amy1, Gsta3*), especially DNA mismatch repair (*Mlh1*), FA metabolism (*Dynlt1b, Gsta3, Cryba4*), and progesterone/estrogen activity (*Gsta3, Cryba4*) (Table S8). For *Mlh1* and *Dynlt1b*, the difference in expression was carried over from the initiation stage (Figure. 4E). This data indicates the association between CD73 activity, FA metabolism, mutational tumor burden, and progesterone signaling in the regulation of mammary gland tumorigenesis.

Interestingly, at the initiation stage down-regulated expression of *Mlh1* was compensated by up-regulation of 10 other genes from GO:0006974 (cellular response to DNA damage stimulus) pathway (Figure 4F, Table S9). PPI analysis generated for the products of these DEGs using the STRING database shows a network consisting mostly of the proteins involved in the DNA repair and stability with Brip1 (BRCA1 interacting protein C-terminal helicase 1) as a connecting node for Mlh1 (part of DNA damage response, DDR). Furthermore, it was accompanied by an up-regulated expression of *the Sesn2* gene, coding Sestrin2, a highly conserved metabolic protein with protective activity against DNA damage, oxidative stress, and hypoxia acting mainly through activation of the key energy sensor and a negative regulator of FAS, AMP-dependent protein kinase (AMPK) [47,48]. Up-regulation of these genes faded out at the progression stage (Fig. S5). Therefore, as the next step, we analyzed MGTs for CD73 KO-induced changes in the expression of MLH1, phosphorylated form of AMPK (p-AMPKα1/2), and phosphorylated form of histone H2AX (γ-H2A.X), an indirect marker of DNA double-strand breaks (DSBs) (Figure 4G). IHC staining showed a significant drop in MLH1 (confirming transcriptome analysis) and p-AMPKα1/2 expression in CD73 KO PR-negative MGTs, while no differences were detected in PR-positive MGTs. However, the level of γ-H2AX was unchanged in all groups with a PR-status-dependent tendency only.

3.5. CD73 regulates DDR and oxidative stress response in a PR- and mutational landscape-dependent context in BC cell lines

Changes in *Mlh1* expression in PR-negative tumors were accompanied by a decreased expression of *Gsta3* at the progression stage (Table S8). Glutathione S-transferase A3 (GSTA3) is an antioxidative protease involved in glutathione-dependent removal of lipid peroxidation products [49]. It indicates a potential role of CD73 in the regulation of mutational burden through the regulation of lipid peroxidation in association with CD73's effect on FA metabolism. Therefore, using human BC cell lines we assessed the impact of CD73 inhibition on the expression of DDR and DSBs markers, oxidative stress, glutathione S-transferase activity, and general levels of reactive oxygen species (ROS) production in correlation with PR expression (Figure 5A,B,C,D Fig S6). Western Blot analysis showed a significant time-dependent decrease in MLH1 levels in PR-negative BC cells after incubation with CD73 inhibitor, AOPCP (Figure 5A), except for the BRCA1 mutant cell line (MDA MB 436). The level of γ-H2A.X increased in both PR-positive and most PR-negative cell lines (increase in 4T1 and MDA MB 436, decrease in MDA MB 231), indicating accumulation of DNA damage induced by CD73 chemical depletion. In the oxidative stress response, we observed a significant overall increase of SOD1 expression in TNBC cell lines, an enzyme that catalyzes superoxide anion radical ($O_2^{\bullet -}$) to oxygen and hydrogen peroxide (H_2O_2), while the level of GPx-1/2 (glutathione peroxidase 1/2), enzyme next in the cascade was not changed. However, we did observe a significant PR-dependent increase in glutathione S-transferase activity (Figure 5C, Fig. S6E), which led to a substantial drop in intracellular levels of ROS (Figure 5D, Fig. S6F).

Some of the results of CD73 depletion on the expression of analyzed DDR and DSB markers indicate the potential interfering effect of the diverse genomic and mutational landscape of BC cell lines. Therefore, we assessed the basal mRNA expression in a panel of selected 48 BC cell lines from CCLE datasets to further analyze the association between *NT5E, PPARG, PGR*, and DEGs specific for PR-negative tumors (specifically *GSTA3* and *MLH1*) in human BC cells. While there was some correlation between CD73 and PPARγ when PR status-based dichotomization was applied, with higher co-expression of *NT5E* and *PPARG* in PR-negative tumors (in agreement with the data from TMAs — Figures 4B), *MLH1* and *GSTA3* were mostly expressed independently of PR status (Figure 5D), similarly as in our murine model (Figure 4E). Next, we assessed these changes at the protein level following chemical depletion of CD73 activity in the cell lines. In normoxic conditions, similar to these at the early stages of tumor development, CD73 inhibition or lack of PR increased PPARγ expression (Figure 4E,F). Similar results were observed in all three applied models (Fig. S7A,B), but the CD73 KO PR-negative MGTs, probably due to the overrepresentation of larger and deeply hypoxic MGTs in our murine model compared to the clinical cohort (Fig. S8A,B). Meanwhile, changes in MLH1 expression were PR-specific, with expression increased in PR-negative controls (identical to WT PR-negative MGTs; Figure 4E,G) and decreased in AOPCP-treated cells (similar to CD73 KO MGs and PR-negative MGTs; Figure 4E,G and Fig. 4A). There were no significant changes in GSTA3 expression following CD73 inhibition, only a PR-status dependent tendency (similar to distribution of ROS production in Figure 5D). However, a more detailed analysis (Figure 9A,B,C) indicates that some intrinsic molecular subtypes of BC are more sensitive to CD73-induced changes, especially Luminal B and Mesenchymal TNBC/TNBC-B.

3.6. CD73 regulates genome stability and TMB in correlation with the HR status of BC patients

To confirm the clinical significance of CD73 depletion-induced changes on genome stability in PR/ER-negative mammary gland tumors, we analyzed data from the METABRIC cohort (Figure 6A). We limited our analysis to the double positive (PR + ER+) and double negative (PR-ER-) tumors to omit the problem connected with the reduced ER expression in our murine model resulting in significant differences in the distribution of hormonal receptors (PR, ER) between analyzed models (Table S10).

We observed differences in the distribution of integrative cluster (IntClust) groups, novel molecular stratification of the breast cancer population derived from the impact of somatic copy number aberrations (CNAs) on the transcriptome [37], according to the PR/ER and *NT5E* status of the patients (Figure 6B). PR/ER status affected the distribution of patients classified to IntClust 1, 2, 3, 4ER+/ER-, 6, 7, 8, and 10 groups, while differences in *NT5E* expression affected their distribution to IntClust 3, 4ER+/ER-, 5, 9, and 10 groups. Analysis of the effect in IntClust 5 (related to the HER2+ patients [37]), shows that PR-ER- groups had a higher percentage of HER2+ patients (*NT5E* high — 28%, *NT5E* low — 22%; HER2+ patients), than the PR + ER + groups (*NT5E* high — 7%, *NT5E* low — 2%; triple positive BC patients). Ultimately, the *NT5E* low PR-ER- group presented decreased incidence in IntClusts with good prognosis and low genome instability (IntClust 3, 4ER+/ER-, 7, 8) and increased in IntClust 10 with

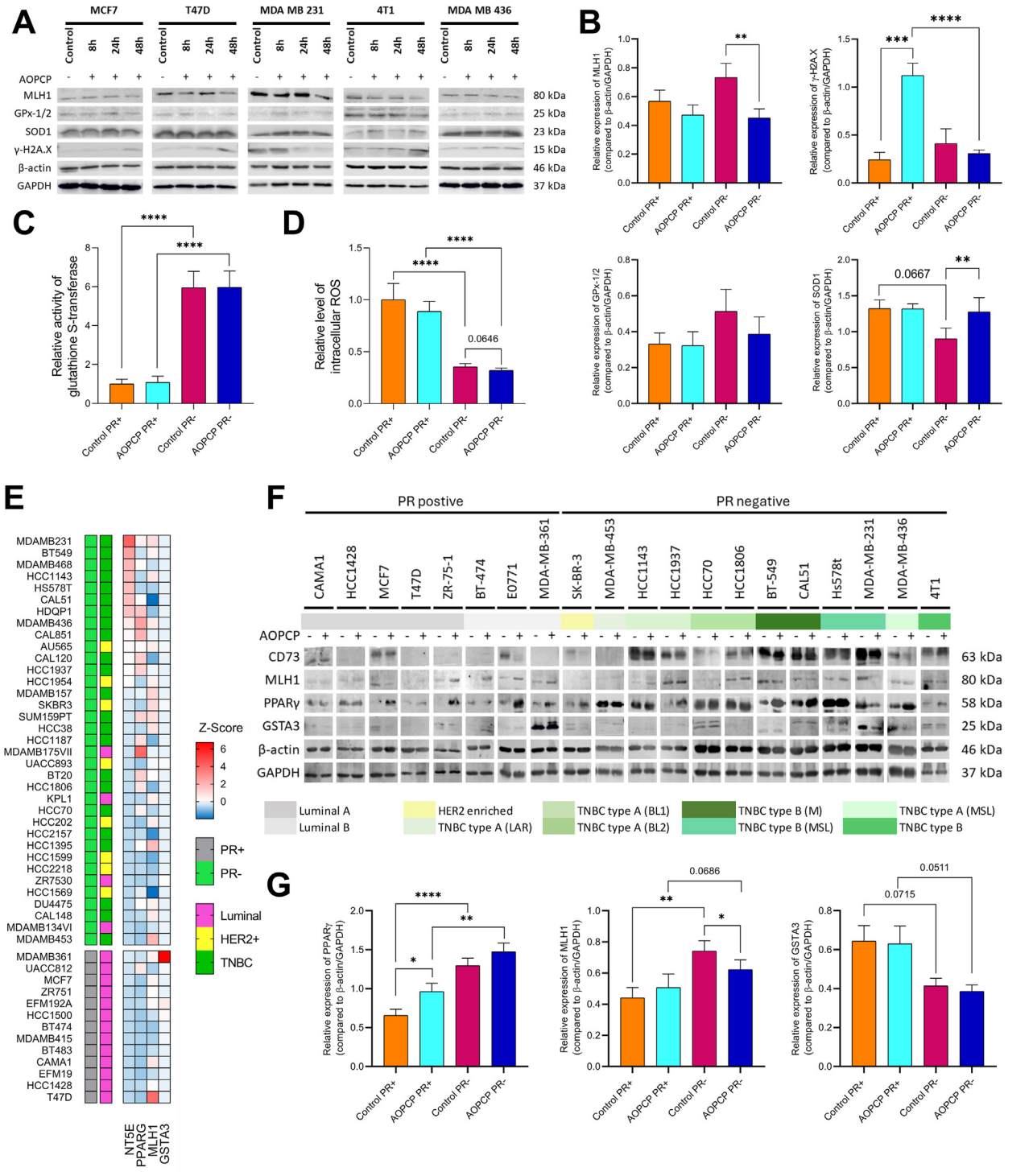

Figure 5: CD73 through reprogrammed lipid metabolism regulates oxidative stress response and tumor mutational burden in association with PR expression. (A) CD73 depletion-induced time-manner changes in MLH1, γ-H2A.X, GPx-1/2, and SOD1 protein expression in BC cell lines treated with AOPCP (CD73 inhibitor). Representative images of western blot analysis of each antigen for each set of conditions. (B) Summarized results of densitometry analysis from 5 cell lines for MLH1, γ-H2A.X, GPx-1/2, and SOD1 after 48h of stimulation (Control vs AOPCP). Mean + SEM. (C) Summary results of the relative activity of glutathione S-transferase *in vitro* from 10 cell lines after 48h of stimulation with AOPCP. Mean + SEM. (C) Summary results of the general level of intracellular ROS production *in vitro* from 9 cell lines after 48h of stimulation with AOPCP, measured by flow cytometry. Mean + SEM. (D) The heatmap of the mRNA expression of *NT5E, PPARG, MLH1, and GSTA3* in 48 BC cell lines from CCLE datasets sorted by *NT5E* expression. (E) CD73 depletion-induced changes of CD73, MLH1, PPARγ, and GSTA3 protein expression in 20 BC cell lines treated with AOPCP for 48h and cultured in normoxia conditions, evaluated by western blot analysis. Representative images of each antigen for each pair of conditions. (F) The changes induced by CD73 inhibition *in vitro* at the protein level of PPARγ, MLH1, and GSTA3. Summary results of densitometry analysis from 20 cell lines. Mean + SEM. ANOVA or Kruskal–Wallis test for multiple comparisons; Paired t-test or Wilcoxon matched-pairs test for paired comparisons; unpaired t-test or Mann–Whitney test for other comparisons. *$p < 0.050$, **$p < 0.010$, ***$p < 0.001$, ****$p < 0.0001$.

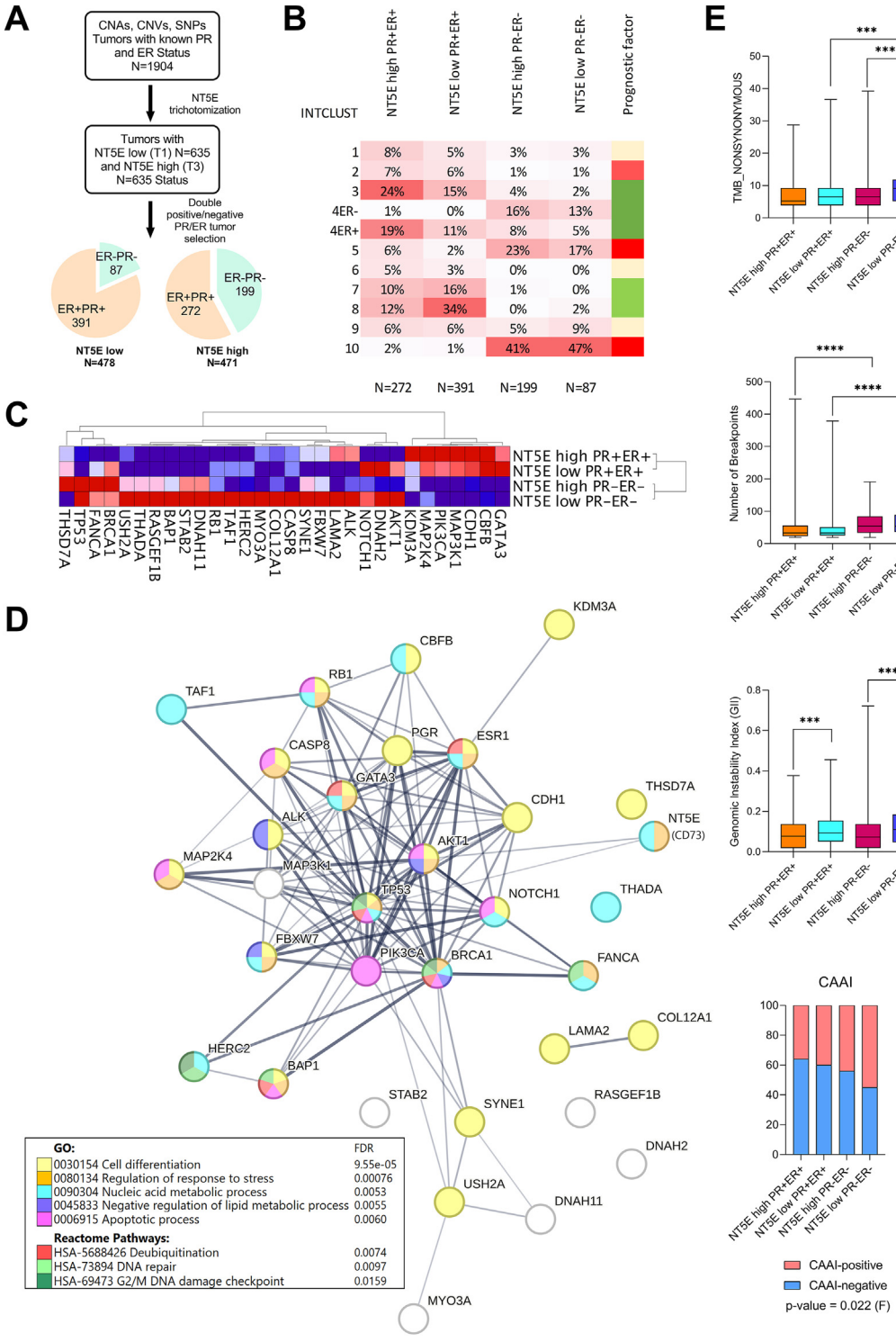

Figure 6: Low CD73 (NT5E) expression increases tumor mutational burden in PR-ER- BC patients. A) Flow chart of human MGTs genome and transcriptome analyses from METABRIC cohort. Patients *NT5E* high/low (*NT5E* high - T1, *NT5E* low - T3) were grouped according to their PR/ER status. B) Distribution of integrative clusters (IntClust) in analyzed groups. Data shows the percentage of patients classified to certain IntClust in a total number of patients. The prognostic value of IntClust: darker red — least favorable, darker green — most favorable, yellow — intermediate value. C) The heatmap of the unsupervised hierarchical clustering of gene mutation profiles in analyzed groups. Only genes with significant differences in frequencies between tested groups were analyzed. Red denotes a higher and blue a lower fraction of mutated samples per group. D) The STRING database-generated visualization of a protein—protein interactions network of protein products of mutated genes involved in cell differentiation, lipid metabolism, DNA repair, and apoptosis. The lines represent text-mining evidence in the PPI network, and their thickness indicates the strength of data support. The bubble colors represent gene involvement in GO terms and Reactome Pathways listed in table. E) Differences in TMB, number of breakpoints, GII, and CAAI in patients grouped according to the *NT5E* and PR/ER status. TMB, number of Breakpoints and GII - Kruskal-Wallis test, ***p $<$ 0.001, ****p $<$ 0.0001, CAAI — Fisher test.

worse prognosis and high genome instability (IntClust 10 is characteristic for basal tumors), suggesting that the *NT5E* low PR-ER- phenotype might be associated with poor survival. The same strong effects of PR/ER and *NT5E* status were observed for the unsupervised hierarchical clustering analysis of the most mutated genes across the analyzed groups of patients (Figure 6C) (Table S11). In the *NT5E* low PR-ER- group, the most mutated genes are involved in nucleic acid and lipid metabolic processes, regulation of response to stress, apoptosis, deubiquitination, DNA repair, and G2/M DNA damage checkpoints (Figure 6D). Next, we analyzed common markers of genome instability and dysregulation of DNA repair. The *NT5E* low PR-ER- group was characterized by the highest tumor mutational burden (TMB), number of DNA breakpoints, genomic instability index (GII), and complex arm-wise aberration index (CAAI) (Figure 6E). The PR/ER status had the most impact on the number of DNA breakpoints (p-value for PR/ER = 4.63E-06; 2-way ANOVA with interactions), while *NT5E* expression affected GII the most (p-value for *NT5E* = 1.01E-03; 2-way ANOVA with interactions) (Table S12). The effect on TMB (p-value for CD73-PR/ER interaction = 1.26E-02; 2-way ANOVA with interactions) and CAAI (p-value for *NT5E*/PR/ER phenotype = 0.02078; Chi-square test) might be a compound effect of both HR-negative and *NT5E* low status. Each of these factors is considered an independent prognostic marker of unfavorable value, that supports our overall hypothesis that low CD73 expression enhances mutational burden through lipid metabolism disruption in correlation with the development of HR-negative tumors.

4. DISCUSSION

Using a murine model of chemically induced mammary gland tumorigenesis, we observed that CD73 genetic depletion delayed the onset of mammary tumors, mainly HR-negative ones (Figure 7). This delay correlated with increased biosynthesis and β-oxidation of fatty acids in the CD73 KO group as indicated by RNA-seq and FA profile. In the CD73 KO group, STRING analysis indicated an interplay between the up-regulated DEGs involved in FA metabolism and increased expression of the gene coding for PR, with PPARγ as a main connective node. We observed a significant association between CD73, PPARγ, and PR in regulating tumor mutational burden in murine and human mammary gland tumors. Our results seem to suggest that low CD73 expression/CD73 KO enhances mutational burden through disruption of lipid metabolism prolonging the onset of more aggressive HR-negative tumors. However, further growth of MGTs was not affected in correlation with a nullifying effect of cancer progression on CD73 KO-induced changes in lipid metabolism.

CD73 KO-induced delay in tumorigenesis was observed for prostate cancer in TRAMP transgenic mice, but it was correlated with the CD73 KO-induced changes in the immune microenvironment [7]. However, for BC we observed this delay to be limited to the HR-negative subtype of MGTs and to correlate with an increased expression of PR at the mRNA level. While PR signaling was shown to have a suppressive role in the pro-oncogenic microenvironment in the prostate at the early stages of tumor development [50], in the murine model of mammary

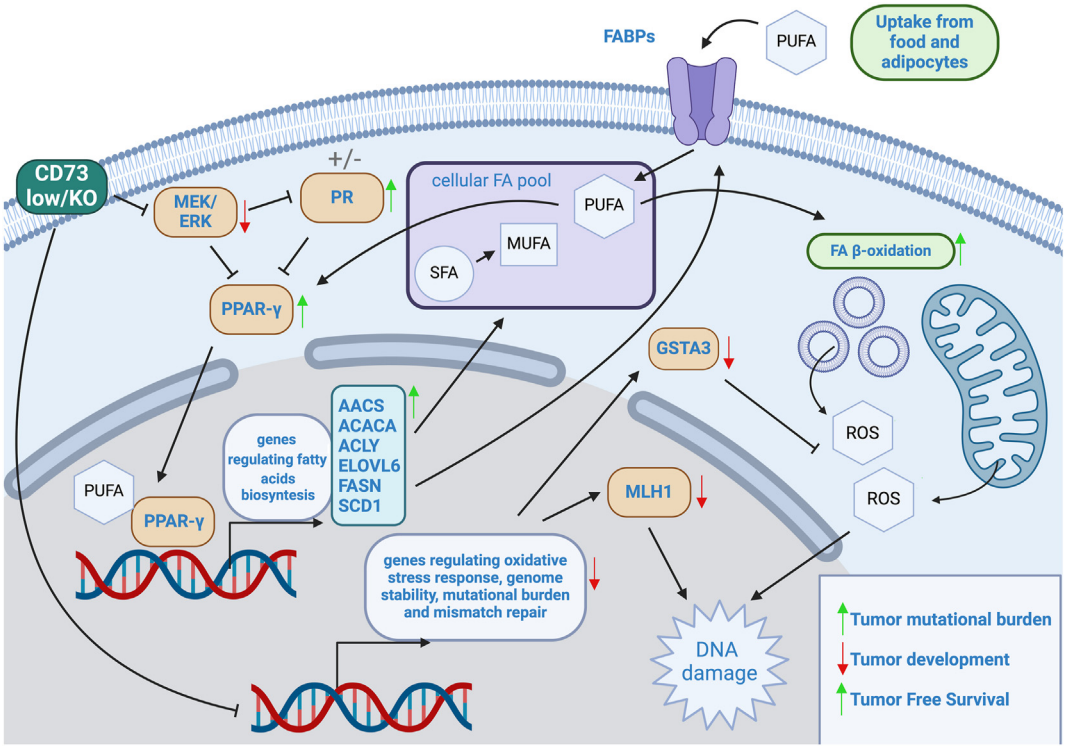

Figure 7: The crucial effect of low CD73 activity on the onset of PR-negative tumors at the early stages of mammary gland tumorigenesis. At the initiation stage, CD73 KO through the MAPK pathway increases Pgr and Pparg expression, inducing an enhanced expression of genes regulating lipid metabolism, including fatty acids biosynthesis and their β-oxidation, resulting in increased percentage of total MUFA and decrease of total PUFAn6. In developing MGTs CD73 KO induces a significant increase in PUFAn6 levels, an important cofactor of PPARγ, creating a positive feedback loop intensifying β-oxidation in peroxisomes and mitochondria, a process correlating with ROS generation and PR expression. CD73 KO downregulates also the expression of genes regulating cellular stress response like *Gsta3* and *Mlh1*, which in correlation with intracellular ROS generation leads to an increased genome instability and TMB in developing PR-negative tumors, lacking the regulatory effect of PR-related signaling. This overall leads to impaired tumor development and longer TFS of more aggressive PR-negative tumors. Created with BioRender.

gland tumorigenesis it was PR ablation that had a protective effect, reducing mammary tumor incidence and their growth [10]. Nevertheless, it was indicated that PR signaling induces paradoxical context-dependent effects on mammary tumorigenesis, both driving BC and being a favorable marker of disease outcome as it is associated with the more differentiated and less aggressive PR-positive tumors [51].

Both ER and PR can modulate abnormal lipid metabolism in BC, which is highly affected by continuous interactions between tumor cells and cancer-associated adipocytes (CAAs). Modulation of lipid metabolism is an important part of metabolic reprogramming during neoplastic cascade. In BC development, the expression of main enzymes involved in *de novo* synthesis of FAs, ACLY (ATP citrate lyase), ACACA (acetyl-CoA carboxylase alpha, ACC1), FASN (FA synthase), and SCD1 (stearoyl-CoA desaturase 1), is usually upregulated resulting in increased levels of SFAs and MUFAs. However, silencing of ER results in decreased expression of ACACA while estradiol induces SCD1 expression in ER-positive cells [12]. During metabolic reprogramming, there is a cooperation between ER and PR signaling. FA metabolism is affected mainly through PR signaling, estrogens target the PI3K/AKT/mTOR pathway and oncogenes, and together they affect glycolysis [52]. As a result, there are significant differences between FA metabolism in cancer subtypes, with TNBC tumors more dependent on the uptake and storage of exogenous FAs than *de novo* synthesis [12–14]. CD73 KO-induced deregulation of lipid metabolism in mammary glands at the initiation stage indicated PPARγ as a main connective node. Furthermore, the correlation between *PPARG/Pparg* and *NT5E/Nt5e* expression was significant for epithelial subsets of cells in murine and human mammary glands, while absent for adipocytes. It indicates, that CD73 KO-induced changes in PPARγ activity affect mainly cell populations undergoing neoplastic transformation into mammary tumors and not their microenvironment, including adipocytes and immune cells.

PPARγ is a transcription factor broadly expressed not only in adipose tissue but also in various epithelial cell types. It regulates the transcription of genes involved in lipid metabolism, including *Pparg/PPARG*, adipocyte differentiation, energy and glucose homeostasis, and oxidative stress response [1,53,54]. Its increased nuclear localization is associated with longer OS of cancer patients, while its cytoplasmic localization is a prognostically unfavorable factor. There is growing evidence that PPARγ acts as a tumor suppressor in BC modulating tumorigenic cascade and cancer progression, through interaction with the IGF system and its down-stream pathways, such as mitogen-activated protein kinase (MAPK), phosphoinositide 3-kinase (PI3K), and the mechanistic target of rapamycin (mTOR) pathways. Through the upregulation of PTEN, PPARγ can inhibit the PI3K/AKT/mTOR pathway activated by ER signaling, as a result inducing growth arrest. On the other hand, ER signaling can repress PPARγ activation, while PPARγ can antagonize progesterone activity by stimulating PR degradation and inhibiting progesterone-induced PR phosphorylation [1,53,55]. It correlates with an increased PPARγ expression and activation in PR-negative MGTs in our model. However, CD73 KO results in its significant down-regulation in cancer cells of PR-negative tumors, but not PR-positive tumors.

PR and PPARγ play opposite roles in the regulation of PI3K/AKT signaling regulating cell proliferation and survival. Furthermore, phosphorylation through the MAPK/ERK1/2 (extracellular regulated kinase 1/2) pathway has a negative role on PPARγ levels [1] and PR levels and activity [11]. Activation of MAPK/ERK1/2 and PI3K/Akt pathways in normal and cancer cells is strongly associated with extracellular adenosine signaling through adenosine receptors. Loss of progesterone receptor was shown to be correlated with adenosine signaling through the PI3K/AKT signaling pathway [56,57]. While in the adult mammary gland PR is expressed in only a fraction of luminal epithelial cells, PR-positive cells can stimulate the proliferation of PR-negative cells in the basal epithelium through paracrine signaling [11]. Thus, the CD73 KO-induced increase in PR expression can indirectly affect developing PR-negative tumors through their microenvironment and sensitize them to the deregulatory effect of CD73 KO/CD73 low expression on lipid metabolism.

Low PR expression in BC is associated with a decrease in *MLH1* (MutL homolog 1 gene) expression, a member of the DNA mismatch repair system, an aberrant DNA mismatch repair, and increased mutational tumor burden [58]. We observed the downregulated expression of genes involved in cellular stress response (*Mlh1*, *Gsta3*) induced by CD73 KO in correlation with the PR-negative phenotype. We observed also a significant CD73-depletion-induced decrease in MLH1 expression in PR-negative MGTs and PR-negative BC cell lines, correlating with the changes in PPARγ expression at the protein level. At the initiation stage of mammary gland tumorigenesis changes in Mlh1 were accompanied by an upregulated network of the genes involved in the DNA repair and stability as indicated by STRING database analysis. MLH1 through its interaction with FANCJ (also known as BRIP1 or BACH1), a DNA helicase, is needed for recovery and restart of replication [59,60]. However, upregulation of these compensatory genes faded out at the progression stage, and in human colorectal cancer MLH1 deficiency was shown to impair tumor growth through increased mutational load [59]. Furthermore, in the METABRIC cohort, low CD73 expression correlated with increased TMB and genomic instability in the PR-negative group. Thus, our results indicate that the activity of oncogenes and genes involved in the regulation of DNA stability is connected to the pathways regulated by PR, PPARγ, and CD73. On the other hand, increased PR signaling in TNBC cell lines was shown to upregulate the expression of genes detrimental to cell proliferation and invasion including many tumor-suppressor genes, but also consistently dampen the genes involved in the maintenance of genomic stability, especially the ones involved in DNA repair [61]. This correlates with CD73 KO-induced delay in the onset of more aggressive PR-negative tumors in our model.

In most of the BC cell lines, we observed a CD73-depletion-induced increase in the expression of γ-H2A.X, a phosphorylated form of histone H2AX, an indirect marker of DNA double-strand breaks (DSBs). Its phosphorylation is a crucial step in the response to DNA damage, as it is required for the assembly of repair factors at the sites of damage, and is a marker of DNA replication stress [62]. However, in mammary glands, we have seen no CD73 KO-induced difference in the expression of γ-H2A.X. On the other hand, we analyzed tumors isolated at the specific endpoint, when they reached over 1 cm in diameter, which is quite a late stage in tumor development and γ-H2A.X was indicated as not the most reliable marker for assessing solid cancer samples [62]. Furthermore, we observed a significant CD73 KO-induced decrease in the expression of p-AMPKα1/2, while AMPKα knockout was shown to enhance H2A.X phosphorylation and DDR, possibly through down-stream effector pathways Chk2/p53-p21(cip1) and Akt-mTOR [63]. AMPK, activated by the energy-replete conditions, inhibits *de novo* synthesis of fatty acids (FAs) and activates their uptake and FAO. It has also a crucial role in regulating antioxidant defense during oxidative stress upregulating the expression of several antioxidant genes [64]. Furthermore, with cancer progression, we observed a CD73 KO-induced increase in the levels of PUFAn3 and PUFAn6, known ligands of PPARγ and a target for the formation of lipid peroxide intermediates, one of the reactive oxygen species [1,2]. We also observed significant, CD73-and PR-dependent changes in the expression of PPARγ, which can regulate an expression of a vast array

of genes involved in the response to oxidative stress, both pro- and antioxidant [54]. Therefore, our results strongly indicate, that CD73 has a significant role in the regulation of tumor mutational burden through the regulation of DNA damage and oxidative stress response modulating lipid metabolism in correlation with PR expression at the early stages of tumorigenesis (Figure. 7).

However, we have also observed a significant effect of PR-status itself on ROS levels and oxidative stress response. Decreased expression of progesterone receptor was shown to correlate with increased ROS levels in tumor cells [65]. Furthermore, in developing tumors hypoxia and reperfusion due to the neoangiogenesis process result in the generation of ROS [66]. CD73 is one of the main regulators of an adaptive response to hypoxia [6]. The hypoxic tumor microenvironment can induce a further metabolic switch stimulating the change from endogenous FA synthesis to increased exogenous FA uptake in developing tumors through inhibition in glucose-based acetyl-CoA generation, a process accompanied by inhibition of the oxygen-dependent FA desaturation [15]. The differences in the expression of genes involved in lipid metabolism and the changes in FA profiles induced by CD73 KO were thus nullified by the development of mammary tumors. As a result, CD73 KO did not affect the tumor growth rate in our model, even when tumors were stratified according to ER/PR expression. Similar results were observed in the analysis of human BCs by Supernat et al. [40], with no correlation between CD73 expression, histological type, lymph node status, grading, and ER/PR status on OS and DFS (disease-free survival). This can explain the differences in the correlation between PPARγ and CD73 expression in murine and human tumors as they significantly differed in their size. Therefore, at the later stage of tumor development, CD73-regulated effects on DDR and oxidative stress can be attenuated by CD73-regulated response to hypoxia.

Furthermore, oncogenes play a critical role in regulating lipid metabolism and metabolic reprogramming, with the most commonly mutated in BC, PIK3CA, and PTEN, participating in the PI3K/AKT signaling axis. In the most aggressive TNBC tumors frequently amplified MYC oncogene can drive FAO in addition to glycolysis to sustain energy requirements for its hyperproliferative activity [13,14]. We have observed in this work a potential effect of diverse genomic and mutational landscape of BC cell lines on the observed results. Especially BRCA1 as it can interact with MLH1 independently of its interactions with FANCJ and its mutation can affect FAS through its interaction with acetyl-CoA carboxylase alpha (ACACA), an enzyme upregulated by CD73 KO at the initiation stage [60,67]. Furthermore, the effect of CD73 depletion on p-AMPKα1/2 activity can be potentially masked by mutations in its downstream effector pathways that include P53 [63].

CD73 activity can be upregulated by hypoxia and inflammation and as a Zn-dependent enzyme, it can be significantly affected by zinc depletion [6]. In the past few years, many highly potent and selective inhibitors of CD73 and adenosine receptors have been developed and applied for clinical trials. However, significant limitations as to their efficiency and selectivity were also demonstrated [3]. There are also new promising approaches in breast cancer therapy targeting lipid metabolism with small molecule agents, modulation of lipid metabolism with natural compounds, PUFA supplementation, or an application of diabetic drugs, such as metformin, which are already investigated in clinical trials for cancer prevention and treatment [2,13]. However, they are still limited in breast cancer by complicated dynamics of its lipidome in correlation with its molecular subtypes. Furthermore, aberrant regulation of lipid metabolism in cancer and its impact on oncogenic signaling pathways in cancer are highly complex affecting its development, progression, therapeutic resistance, and recurrence [12,13,16]. As a result, PPARγ's role as a BC suppressor demonstrated in preclinical studies did not translate well into human clinical trials with the failure of synthetic PPARγ ligands as to their effectiveness and safety profile [53]. Furthermore, progesterone emerges as the primary mitogen in the adult breast with clinical evidence suggesting that progestins can increase BC risk in part by driving its proliferation at the early stage of development [11]. Therefore, elucidation of the connection between the deregulation of lipid metabolism, oncogenic signaling, and one of the major pathways in cancer progression, the CD73/adenosine axis, gives us a new insight into the process of BC tumorigenesis, especially in the context of breast cancer molecular heterogeneity. A better understanding of this complicated relationship is needed to improve the efficiency of anti-cancer therapies targeted against the CD73-adenosine axis or lipid metabolism.

Our study was limited by a high fraction of ER-negative MGTs in a murine model. We observed significant differences in the distribution of tumors with different combined PR/ER statuses in applied models, especially in the METABRIC cohort, where the number of PR + ER- tumors was negligible (Table S13). Therefore, we excluded single-receptor-positive tumors from further analyses. Despite those evident differences in applied models, we could capture the association between CD73 deficiency and remodeled FA metabolism, increased TMB, and impaired tumor development in association with HR-negative BC. Interestingly, analysis of PR/ER combinations in METABRIC patients showed significant differences in their distribution between *NT5E* high and *NT5E* low groups. Low *NT5E* expression correlated with a higher incidence of PR + ER + tumors (86%−14%, Fisher test <0.0001). It is possible, that in the *NT5E* low PR-ER- group, similarly to the murine model we presented, increased TMB might lead to slower tumor development, explaining a significantly smaller size of this group. It also highlights potential targets for the combined anti-CD73 therapy with checkpoint inhibitors such as anti-PD-1 mAb [3]. Evidence suggests that TMB can predict the efficacy of immune checkpoint inhibitors as demonstrated by recently FDA-approved pembrolizumab treatment for the TMB-high tumor subgroup [68].

Our study was also limited by the low incidence of HER2 tumors ($n = 5$ for WT and $n = 3$ for CD73 KO mice). In the METABRIC cohort, we observed a significant decrease in HER2+ tumor incidence in CD73 low patients (6%, 28/478) compared to CD73 high group (16%, 75/396, Fisher test <0.0001). In our murine model, we saw that only as a weak tendency, and the PPARγ was not activated (data not shown). Therefore, further study on a larger group of mice is required to elucidate the effect of CD73 expression on latency, incidence, and FA metabolism of HER2+ tumors.

5. CONCLUSIONS

Our results demonstrate a significant and novel role of CD73 in the regulation of metabolic reprogramming of lipid metabolism during mammary gland tumorigenesis. We show CD73 in a regulatory loop with PR and PPARγ in epithelial cells undergoing neoplastic transformation. Its deregulation, by genetic knock-out, inhibition, or the low expression of CD73, disturbs this process, especially in PR-negative tumors with their specific metabolic requirements. As a result, TNBC tumors have their onset delayed, but their genomic instability and tumor mutational burden seem to be increased in correlation with their more aggressive phenotype.

FUNDING SOURCES

This work was supported by the grant 2017/27/B/NZ5/02192 to PK from the National Science Centre (www.ncn.gov.pl), from grant 664/73-3306/63/351 to PKS from the Medical University of Gdańsk, and from grant 71-01424/K16 0007669 to WL from the Medical University of Gdańsk. Equipment used to scan IHC was maintained with funds from the Ministry of Science and Higher Education, grant 2/566516/SPUB/SP/2023. The funders had no role in study design, data collection and analysis, decision to publish, or preparation of the manuscript.

CREDIT AUTHORSHIP CONTRIBUTION STATEMENT

Paweł Kamil Serafin: Writing — original draft, Visualization, Validation, Supervision, Software, Methodology, Investigation, Formal analysis, Data curation, Conceptualization, Funding acquisition. **Marta Popęda:** Writing — review & editing, Validation, Resources, Methodology, Investigation, Formal analysis. **Kamila Bulak:** Writing — review & editing, Visualization, Resources, Methodology, Investigation, Formal analysis. **Agata Zwara:** Writing — review & editing, Investigation. **Barbara Galikowska-Bogut:** Writing — review & editing, Visualization, Methodology, Investigation, Formal analysis. **Anna Przychodzka:** Writing — review & editing, Visualization, Methodology, Investigation, Formal analysis. **Adriana Mika:** Writing — review & editing, Resources, Methodology, Investigation, Formal analysis, Conceptualization. **Tomasz Śledziński:** Writing — review & editing, Resources, Formal analysis. **Marcin Stanisławowski:** Writing — review & editing, Resources, Methodology, Investigation. **Kamila Jendernalik:** Writing — review & editing, Resources, Investigation. **Marika Bolcewicz:** Writing — review & editing, Resources, Investigation. **Wiktoria Laprus:** Writing — review & editing, Resources, Methodology, Investigation, Formal analysis, Funding acquisition. **Grzegorz Stasiłojć:** Writing — review & editing, Methodology, Investigation, Formal analysis. **Rafał Sądej:** Writing — review & editing, Supervision, Resources. **Anna Żaczek:** Writing — review & editing, Supervision, Resources, Data curation. **Leszek Kalinowski:** Writing — review & editing, Supervision, Resources, Funding acquisition. **Patrycja Koszałka:** Writing — original draft, Visualization, Validation, Supervision, Software, Resources, Project administration, Methodology, Investigation, Funding acquisition, Formal analysis, Conceptualization.

ACKNOWLEDGMENTS

We would like to thank Kamil Myszczyński for performing the bioinformatics analysis and Adam Wyszomirski for providing biostatistics consultation within the services of the Centre of Biostatistics and Bioinformatics Analysis, Medical University of Gdańsk, Poland. The Centre is working as part of "Excellence Initiative — Research University" grant No. MNiSW 07/IDUB/2019/94.

DECLARATION OF COMPETING INTEREST

None.

DATA AVAILABILITY

Data will be made available on request.

APPENDIX A. SUPPLEMENTARY DATA

Supplementary data to this article can be found online at https://doi.org/10.1016/j.molmet.2024.102035.

REFERENCES

[1] Zhao B, Xin Z, Ren P, Wu H. The role of PPARs in breast cancer. Cells 2022;12(1):130. https://doi.org/10.3390/cells12010130.
[2] Zhang C, Zhu N, Li H, Gong Y, Gu J, Shi Y, et al. New dawn for cancer cell death: emerging role of lipid metabolism. Mol Metabol 2022;63:101529. https://doi.org/10.1016/j.molmet.2022.101529.
[3] Kutryb-Zając B, Kawecka A, Nasadiuk K, Braczko A, Stawarska K, Caiazzo E, et al. Drugs targeting adenosine signaling pathways: a current view. Biomed Pharmacother 2023;165:115184. https://doi.org/10.1016/j.biopha.2023.115184.
[4] Allard B, Allard D, Buisseret L, Stagg J. The adenosine pathway in immuno-oncology. Nat Rev Clin Oncol 2020;17(10):611—29. https://doi.org/10.1038/s41571-020-0382-2.
[5] Antonioli L, Fornai M, Pellegrini C, D'Antongiovanni V, Turiello R, Morello S, et al. Adenosine signaling in the tumor microenvironment. In: Birbrair A, editor. Tumor microenvironment, vol. 1270. Cham: Springer International Publishing; 2021. p. 145—67.
[6] Zimmermann H. History of ectonucleotidases and their role in purinergic signaling. Biochem Pharmacol 2021;187:114322. https://doi.org/10.1016/j.bcp.2020.114322.
[7] Stagg J, Beavis PA, Divisekera U, Liu MCP, Möller A, Darcy PK, et al. CD73-Deficient mice are resistant to carcinogenesis. Cancer Res 2012;72(9):2190—6. https://doi.org/10.1158/0008-5472.CAN-12-0420.
[8] Wang R, Zhang Y, Lin X, Gao Y, Zhu Y. Prognositic value of CD73-adenosinergic pathway in solid tumor: a meta-analysis and systematic review. Oncotarget 2017;8(34):57327—36. https://doi.org/10.18632/oncotarget.16905.
[9] Yager JD, Davidson NE. Estrogen carcinogenesis in breast cancer. N Engl J Med 2006;354(3):270—82. https://doi.org/10.1056/NEJMra050776.
[10] Lydon JP, Ge G, Kittrell FS, Medina D, O'Malley BW. Murine mammary gland carcinogenesis is critically dependent on progesterone receptor function. Cancer Res 1999;59(17):4276—84.
[11] Cenciarini ME, Proietti CJ. Molecular mechanisms underlying progesterone receptor action in breast cancer: insights into cell proliferation and stem cell regulation. Steroids 2019;152:108503. https://doi.org/10.1016/j.steroids.2019.108503.
[12] Monaco ME. Fatty acid metabolism in breast cancer subtypes. Oncotarget 2017;8(17):29487—500. https://doi.org/10.18632/oncotarget.15494.
[13] Ward AV, Anderson SM, Sartorius CA. Advances in analyzing the breast cancer lipidome and its relevance to disease progression and treatment. J Mammary Gland Biol Neoplasia 2021;26(4):399—417. https://doi.org/10.1007/s10911-021-09505-3.
[14] Zhao C, Wu M, Zeng N, Xiong M, Hu W, Lv W, et al. Cancer-associated adipocytes: emerging supporters in breast cancer. J Exp Clin Cancer Res 2020;39(1):156. https://doi.org/10.1186/s13046-020-01666-z.
[15] Munir R, Lisec J, Swinnen JV, Zaidi N. Lipid metabolism in cancer cells under metabolic stress. Br J Cancer 2019;120(12):1090—8. https://doi.org/10.1038/s41416-019-0451-4.
[16] Bian X, Liu R, Meng Y, Xing D, Xu D, Lu Z. Lipid metabolism and cancer. J Exp Med 2021;218(1):e20201606. https://doi.org/10.1084/jem.20201606.
[17] Thom VT, Wendel M, Deussen A. Regulation of ecto-5'-nucleotidase by docosahexaenoic acid in human endothelial cells. Cell Physiol Biochem 2013;32(2):355—66. https://doi.org/10.1159/000354443.

[18] Müller G, Jung C, Wied S, Biemer-Daub G, Frick W. Transfer of the glycosylphosphatidylinositol-anchored 5′-nucleotidase CD73 from adiposomes into rat adipocytes stimulates lipid synthesis: intercellular transfer of GPI-proteins. Br J Pharmacol 2010;160(4):878–91. https://doi.org/10.1111/j.1476-5381.2010.00724.x.

[19] Burghoff S, Flögel U, Bongardt S, Burkart V, Sell H, Tucci S, et al. Deletion of CD73 promotes dyslipidemia and intramyocellular lipid accumulation in muscle of mice. Arch Physiol Biochem 2013;119(2):39–51. https://doi.org/10.3109/13813455.2012.755547.

[20] Liu Y, Yin T, Feng Y, Cona MM, Huang G, Liu J, et al. Mammalian models of chemically induced primary malignancies exploitable for imaging-based preclinical theragnostic research. Quant Imag Med Surg 2015;5(5):708–29. https://doi.org/10.3978/j.issn.2223-4292.2015.06.01.

[21] Kilkenny C, Browne W, Cuthill IC, Emerson M, Altman DG. Animal research: reporting *in vivo* experiments: the ARRIVE guidelines. Br J Pharmacol 2010;160(7):1577–9. https://doi.org/10.1111/j.1476-5381.2010.00872.x.

[22] Koszalka P, Özüyaman B, Huo Y, Zernecke A, Flögel U, Braun N, et al. Targeted disruption of *cd73*/Ecto-5′-Nucleotidase alters thromboregulation and augments vascular inflammatory response. Circ Res 2004;95(8):814–21. https://doi.org/10.1161/01.RES.0000144796.82787.6f.

[23] Cardiff RD, Anver MR, Gusterson BA, Hennighausen L, Jensen RA, Merino MJ, et al. The mammary pathology of genetically engineered mice: the consensus report and recommendations from the Annapolis meeting. Oncogene 2000;19(8):968–88. https://doi.org/10.1038/sj.onc.1203277.

[24] R Core Team. R: a language and environment for statistical computing. R: a language and environment for statistical computing. Vienna, Austria: R Foundation for Statistical Computing; 2021. https://www.r-project.org/. [Accessed 11 April 2022].

[25] Andrews S, Krueger F, Seconds-Pichon A, Biggins F, Wingett S. FastQC. A quality control tool for high throughput sequence data 2015;1(1):1.

[26] Bolger AM, Lohse M, Usadel B. Trimmomatic: a flexible trimmer for Illumina sequence data. Bioinformatics 2014;30(15):2114–20. https://doi.org/10.1093/bioinformatics/btu170.

[27] Dobin A, Davis CA, Schlesinger F, Drenkow J, Zaleski C, Jha S, et al. STAR: ultrafast universal RNA-seq aligner. Bioinformatics 2013;29(1):15–21. https://doi.org/10.1093/bioinformatics/bts635.

[28] Liao Y, Smyth GK, Shi W. featureCounts: an efficient general purpose program for assigning sequence reads to genomic features. Bioinformatics 2014;30(7):923–30. https://doi.org/10.1093/bioinformatics/btt656.

[29] Love MI, Huber W, Anders S. Moderated estimation of fold change and dispersion for RNA-seq data with DESeq2. Genome Biol 2014;15(12):550. https://doi.org/10.1186/s13059-014-0550-8.

[30] Alexa A, Rahnenfuhrer J. TopGO: enrichment analysis for gene ontology. R Package version 2022;2.48.0. n.d.

[31] Carlson M. org.Mm.eg.db: genome wide annotation for Mouse. R package version 2019;3.8.2.

[32] Szklarczyk D, Franceschini A, Wyder S, Forslund K, Heller D, Huerta-Cepas J, et al. STRING v10: protein–protein interaction networks, integrated over the tree of life. Nucleic Acids Res 2015;43(D1):D447–52. https://doi.org/10.1093/nar/gku1003.

[33] Folch J, Lees M, Stanley GHS. A simple method for the isolation and purification of total lipides from animal tissues. J Biol Chem 1957;226(1):497–509. https://doi.org/10.1016/S0021-9258(18)64849-5.

[34] Mika A, Kobiela J, Pakiet A, Czumaj A, Sokołowska E, Makarewicz W, et al. Preferential uptake of polyunsaturated fatty acids by colorectal cancer cells. Sci Rep 2020;10(1):1954. https://doi.org/10.1038/s41598-020-58895-7.

[35] Reich M, Liefeld T, Gould J, Lerner J, Tamayo P, Mesirov JP. GenePattern 2.0. Nat Genet 2006;38(5):500–1. https://doi.org/10.1038/ng0506-500.

[36] Sherman BT, Hao M, Qiu J, Jiao X, Baseler MW, Lane HC, et al. DAVID: a web server for functional enrichment analysis and functional annotation of gene lists (2021 update). Nucleic Acids Res 2022;50(W1):W216–21. https://doi.org/10.1093/nar/gkac194.

[37] Metabric Group, Curtis C, Shah SP, Chin S-F, Turashvili G, Rueda OM, et al. The genomic and transcriptomic architecture of 2,000 breast tumours reveals novel subgroups. Nature 2012;486(7403):346–52. https://doi.org/10.1038/nature10983.

[38] Emont MP, Jacobs C, Essene AL, Pant D, Tenen D, Colleluori G, et al. A single cell atlas of human and mouse white adipose tissue. Physiology 2021;603(7903):926–33. https://doi.org/10.1038/s41586-022-04518-2.

[39] Gray GK, Li CM-C, Rosenbluth JM, Selfors LM, Girnius N, Lin J-R, et al. A human breast atlas integrating single-cell proteomics and transcriptomics. Dev Cell 2022;57(11):1400–1420.e7. https://doi.org/10.1016/j.devcel.2022.05.003.

[40] Supernat A, Markiewicz A, Wełnicka-Jaśkiewicz M, Seroczyńska B, Skokowski J, Sejda A, et al. CD73 expression as a potential marker of good prognosis in breast carcinoma. Appl Immunohistochem Mol Morphol 2012;20(2):103–7. https://doi.org/10.1097/PAI.0b013e3182311d82.

[41] Dall GV, Hawthorne S, Seyed-Razavi Y, Vieusseux J, Wu W, Gustafsson J-A, et al. Estrogen receptor subtypes dictate the proliferative nature of the mammary gland. J Endocrinol 2018;237(3):323–36. https://doi.org/10.1530/JOE-17-0582.

[42] Campbell EJ, Tesson M, Doogan F, Mohammed ZM, Mallon E, Edwards J. The combined endocrine receptor in breast cancer, a novel approach to traditional hormone receptor interpretation and a better discriminator of outcome than ER and PR alone. Br J Cancer 2016;115(8):967–73. https://doi.org/10.1038/bjc.2016.206.

[43] Yu K, Cai Y, Wu S, Shui R, Shao Z. Estrogen receptor-low breast cancer: biology chaos and treatment paradox. Cancer Commun 2021;41(10):968–80. https://doi.org/10.1002/cac2.12191.

[44] Matsuzaka T, Shimano H. Elovl6: a new player in fatty acid metabolism and insulin sensitivity. J Mol Med 2009;87(4):379–84. https://doi.org/10.1007/s00109-009-0449-0.

[45] Berryhill GE, Trott JF, Hovey RC. Mammary gland development—it's not just about estrogen. J Dairy Sci 2016;99(1):875–83. https://doi.org/10.3168/jds.2015-10105.

[46] Wongtangtintharn S, Oku H, Iwasaki H, Toda T. Effect of branched-chain fatty acids on fatty acid biosynthesis of human breast cancer cells. J Nutr Sci Vitaminol 2004;50(2):137–43. https://doi.org/10.3177/jnsv.50.137.

[47] Chen Y, Huang T, Yu Z, Yu Q, Wang Y, Hu J, et al. The functions and roles of sestrins in regulating human diseases. Cell Mol Biol Lett 2022;27(1):2. https://doi.org/10.1186/s11658-021-00302-8.

[48] Wang Q, Liu S, Zhai A, Zhang B, Tian G. AMPK-mediated regulation of lipid metabolism by phosphorylation. Biol Pharm Bull 2018;41(7):985–93. https://doi.org/10.1248/bpb.b17-00724.

[49] Yang Y. Role of α class glutathione S-transferases as antioxidant enzymes in rodent tissues. Toxicol Appl Pharmacol 2002;182(2):105–15. https://doi.org/10.1006/taap.2002.9450.

[50] Chen R, Yu Y, Dong X. Progesterone receptor in the prostate: a potential suppressor for benign prostatic hyperplasia and prostate cancer. J Steroid Biochem Mol Biol 2017;166:91–6. https://doi.org/10.1016/j.jsbmb.2016.04.008.

[51] Hilton HN, Clarke CL, Graham JD. Estrogen and progesterone signalling in the normal breast and its implications for cancer development. Mol Cell Endocrinol 2018;466:2–14. https://doi.org/10.1016/j.mce.2017.08.011.

[52] Ward AV, Matthews SB, Fettig LM, Riley D, Finlay-Schultz J, Paul KV, et al. Estrogens and progestins cooperatively shift breast cancer cell metabolism. Cancers 2022;14(7):1776. https://doi.org/10.3390/cancers14071776.

[53] Augimeri G, Bonofiglio D. PPARgamma: a potential intrinsic and extrinsic molecular target for breast cancer therapy. Biomedicines 2021;9(5):543. https://doi.org/10.3390/biomedicines9050543.

[54] Polvani S, Tarocchi M, Galli A. PPAR and oxidative stress: con catenating NRF2 and FOXO. PPAR Res 2012;2012:1–15. https://doi.org/10.1155/2012/641087.

[55] Wang P, Dharmaraj N, Brayman MJ, Carson DD. Peroxisome proliferator-activated receptor γ activation inhibits progesterone-stimulated human

MUC1 expression. Mol Endocrinol 2010;24(7):1368–79. https://doi.org/10.1210/me.2009-0221.

[56] Fishman P, Bar-Yehuda S, Synowitz M, Powell JD, Klotz KN, Gessi S, et al. Adenosine receptors and cancer. In: Wilson CN, Mustafa SJ, editors. Adenosine receptors in health and disease, vol. 193. Berlin, Heidelberg: Springer Berlin Heidelberg; 2009. p. 399–441.

[57] Tahiri A, Tekpli X, Satheesh SV, DeWijn R, Lüders T, Bukholm IR, et al. Loss of progesterone receptor is associated with distinct tyrosine kinase profiles in breast cancer. Breast Cancer Res Treat 2020;183(3):585–98. https://doi.org/10.1007/s10549-020-05763-7.

[58] Cheng AS, Leung SCY, Gao D, Burugu S, Anurag M, Ellis MJ, et al. Mismatch repair protein loss in breast cancer: clinicopathological associations in a large British Columbia cohort. Breast Cancer Res Treat 2020;179(1):3–10. https://doi.org/10.1007/s10549-019-05438-y.

[59] Germano G, Lamba S, Rospo G, Barault L, Magrì A, Maione F, et al. Inactivation of DNA repair triggers neoantigen generation and impairs tumour growth. Nature 2017;552(7683):116–20. https://doi.org/10.1038/nature24673.

[60] Cantor SB, Xie J. Assessing the link between BACH1/FANCJ and MLH1 in DNA crosslink repair. Environ Mol Mutagen 2010;51(6):500–7. https://doi.org/10.1002/em.20568.

[61] Leo JCL, Wang SM, Guo CH, Aw SE, Zhao Y, Li JM, et al. Gene regulation profile reveals consistent anticancer properties of progesterone in hormone-independent breast cancer cells transfected with progesterone receptor. Int J Cancer 2005;117(4):561–8. https://doi.org/10.1002/ijc.21186.

[62] Fragkos M, Choleza M, Papadopoulou P. The role of γH2AX in replication stress-induced carcinogenesis: possible links and recent developments. Cancer Diagnosis & Prognosis 2023;3(6):639–48. https://doi.org/10.21873/cdp.10266.

[63] Sanli T, Storozhuk Y, Linher-Melville K, Bristow RG, Laderout K, Viollet B, et al. Ionizing radiation regulates the expression of AMP-activated protein kinase (AMPK) in epithelial cancer cells. Radiother Oncol 2012;102(3):459–65. https://doi.org/10.1016/j.radonc.2011.11.014.

[64] Steinberg GR, Hardie DG. New insights into activation and function of the AMPK. Nat Rev Mol Cell Biol 2023;24(4):255–72. https://doi.org/10.1038/s41580-022-00547-x.

[65] Fallahi N, Rafiee M, Azaryan E, Wilkinson D, Bagheri V. Inhibitory effects of progesterone on the human acute lymphoblastic leukemia cell line. Gene Reports 2024;36:101991. https://doi.org/10.1016/j.genrep.2024.101991.

[66] Brown NS, Bicknell R. Hypoxia and oxidative stress in breast cancer Oxidative stress - its effects on the growth, metastatic potential and response to therapy of breast cancer. Breast Cancer Res 2001;3(5):323. https://doi.org/10.1186/bcr315.

[67] Moreau K, Dizin E, Ray H, Luquain C, Lefai E, Foufelle F, et al. BRCA1 affects lipid synthesis through its interaction with acetyl-CoA carboxylase. J Biol Chem 2006;281(6):3172–81. https://doi.org/10.1074/jbc.M504652200.

[68] Barroso-Sousa R, Pacífico JP, Sammons S, Tolaney SM. Tumor mutational burden in breast cancer: current evidence, challenges, and opportunities. Cancers 2023;15(15):3997. https://doi.org/10.3390/cancers15153997.

